




FACULTY OF SCIENCE AND TECHNOLOGY

MASTER'S THESIS

Study programme / specialisation: Biological Chemistry	<i>Spring semester, 2023</i> Open / Confidential
Author: Scott George Paul	
Supervisor at UiS: Hanne R. Hagland Co-supervisor: External supervisor(s):	
Thesis title: A Bioprinting Workflow for Live Cell Imaging and Mechanical Testing	
Credits (ECTS): 60	
Keywords:	Pages: 62 + appendix: 7 Stavanger, 11 th June 2023

UNIVERSITY OF STAVANGER
MASTERS THESIS

A Bioprinting Workflow for Live Cell Imaging and Mechanical Testing

Scott Paul, BSc

A thesis submitted in partial fulfilment for the degree of Master of
Science in Biological Chemistry

Department of Mathematics and Natural Sciences Faculty of Science
and Technology

Faculty Supervisor: Hanne R. Hagland



University of
Stavanger

Rogaland, Norway

June 2023

Abstract

Bioprinting, an emergent field bridging biology, chemistry and 3D printing technology offers to researchers innovative solutions to progress the study of tissue engineering, drug testing and cellular studies. This thesis presents a novel workflow for the live cell imaging and mechanical testing of 3D bioprinted constructs.

The workflow begins with cultivating PANC-1 cells in standard cell culture flasks or alternatively using 3D culture methods, such as hanging drops or spheroid culture plates. The cells are then encapsulated in one of two different hydrogel environments: Laminink 411, a product from CELLINK, composed of gelatin functionalised with methacrylate groups, alginate and several laminins; or a 3 mg/mL collagen solution made from TeloCol®-10. Laminink encapsulations were printed in the BIO X bioprinter whereas the collagen constructs were formed with the use of a mold. Laminink-PANC-1 hydrogels are solidified using ultra-violet (UV) and ionic crosslinking with CaCl_2 before incubation, while collagen constructs are crosslinked by exposure to 37 °C in an incubator. All hydrogel constructs were formed in Ibidi 35 mm imaging μ -dishes. Post-incubation, cell viability was assessed on a Leica SP8 microscope, using a dual fluorescence stain of calcein green and mitotracker red. Subsequent to imaging, mechanical testing was performed at earliest convenience. Hydrogels were taken to a Discovery HR 20 Hybrid Rheometer (DHR-2) where oscillation amplitude and frequency sweep measurements of the samples were taken.

An advantage of this workflow is that it offers a repeatable process to allow ongoing imaging and mechanical testing. Laminink hydrogels exhibited a resilient, non-degradable nature which allowed the imaging and mechanical workflow to be repeated after a second period of incubation. The results of the study revealed high cell viability for both Laminink and collagen hydrogels, as demonstrated by the confocal images, and the matrix stiffness of the constructs was determined through the Rheometry data obtained. In addition, utilization of the Raise3D Pro 2 and Formlabs 3+ 3D printers were essential to overcome technical challenges in the progress of this thesis. Specifically, they were used to design calibration plates for the BIO X, molds for collagen hydrogel crosslinking and producing static helix mixers to assist in the homogeneous encapsulation of cells within hydrogel networks.

In conclusion, the workflow presented demonstrates an advancement in the merging of advanced 3D bioprinting technology with biological and chemical explorations, broadening the positive future in biomedical research.

Contents

Abstract.....	i
Acknowledgements.....	vii
Declaration	viii
Introduction	1
1.1 Pancreatic Cancer	1
1.2 2D & 3D Cancer Models.....	3
1.3 Bioprinting in Cancer Research.....	4
1.4 Bioprinting Principles	5
1.5 Hydrogel Networks.....	7
1.5.1 Matrigel.....	9
1.5.2 Laminink 411.....	9
1.5.3 Alginate	10
1.5.4 Collagen.....	10
1.6 Live Cell Imaging & Confocal Microscopy.....	11
1.7 Mechanical Testing & Rheology.....	12
1.8 Aims and Objectives.....	13
Materials and Methods	14
2.1 Materials.....	14
2.1.1 Cell Lines.....	14
2.1.2 Reagents.....	15
2.1.3 Prepared Solutions.....	16
2.1.3.1 Complete Cell Media (cDMEM).....	16
2.1.3.2 Imaging Solution.....	16
2.1.3.3 HCl (3.7 %).....	17
2.1.3.4 HEPES (100 mM)	17
2.1.3.5 NaOH (5N and 0.5N)	18

2.1.3.6 Collagen Gel (3 mg/mL)	18
2.1.4 Consumables	19
2.1.5 Instruments	19
2.2 Methods.....	20
2.2.1 2D Cell Preparation	20
2.2.3 Microwell 3D Spheroid Preparation	21
2.2.4 3D Designs and Slicer Settings	21
2.2.4.1 Construct for Cell Viability and Viscoelasticity Testing	22
2.2.4.2 Calibration Plates & Collagen Mold	23
2.2.4.3 Static Mixer Helix & 1 mL End Cap	24
2.2.5 Bioprinting.....	26
2.2.6 Live Cell Imaging	28
2.2.7 Characterisation of Mechanical Properties.....	28
2.2.8 Data Analysis.....	30
Results	31
3.1 Laminink Hydrogels	31
3.1.1 Bioprinted Construct for Cell Viability and Viscoelasticity Testing	31
3.1.2 CELLINK Recommended Settings.....	32
3.1.4 Getting Closer to 4 kPa.....	34
3.1.5 2D PANC-1 Encapsulation	34
3.1.6 Hanging Drop Spheroids Encapsulation	36
3.1.7 Microwell Spheroids Encapsulation.....	36
3.2 Collagen Hydrogels.....	37
Discussion	39
4.1 Summary and Interpretation of Results.....	39
4.2 Bioprinting Optimisations.....	41
4.4 Future Considerations.....	44
Conclusion	48
References	49
Appendix.....	52

List of Figures

1.1 PDAC and the surrounding dense fibrotic tissue	2
1.2 2D and 3D cell culture differences.....	3
1.3 The BIO X 3D Bioprinter from CELLINK.....	4
1.4 Extrusion- and light-based methods for 3D printing	6
1.5 A 3 mL Laminink 411 cartridge and CaCl ₂ crosslinking solution produced by CELLINK.....	9
2.1 Bioprinted construct design process.....	23
2.2 Calibration plate and collagen mold design process.	24
2.3 Static mixer design process	25
2.4 Bioprinting apparatus	27
2.5 Live cell imaging equipment used	28
2.6 Mechanical testing equipment used	29
3.1 Oscillation amplitude results of Laminink rheology disc	31
3.2 Laminink frequency sweep results with 405 nm crosslinking.....	32
3.3 Image of viable PANC-1 cells on day 1 (A) and day 7 (B) in a Laminink hydrogel construct bioprinted using the BIO X.....	35
3.4 A: Surface area scan of an Ibidi 35 mm μ -Dish containing microwell plate PANC-1 spheroids in Laminink 411	36
3.5 Averaged oscillation amplitude and frequency sweep test results of 3 collagen hydrogels.....	37
1 Collagen hydrogel calculation example.....	52
2 Cell solution volume calculation	52
3 Optoelectrical parameters of BIO X 405 nm UV module at 60 mm nominal distance to surface	53

4 Radiation diagram of BIO X 405 nm UV module	53
5 BIO X 405 nm beam diameters at 4.0, 6.0 and 6.5 cm height	54
6 BIO X 405 nm beams created in Blender at 4.0, 6.0 and 6.5 cm module height	54
7 Beam surface area on BIO X with beam angles of 8 and 16 degrees	55
8 Intensity of emitted light as a function of degree angle.	55
9 Relating beam angle, intensity and surface area	56
10 Relationship between 405 nm UV module height and light intensity	56

List of Tables

2.1 PANC-1 cell culture line ATCC No. and details	14
2.2 Reagents, associated manufacturer, reference numbers and purpose	15
2.3 A list of consumables, associated manufacturer and purpose	19
2.4 A list of instruments, associated manufacturer and purpose.....	19
2.5 CELLINK HeartWare slicer settings.....	22
2.6 ideaMaker slicer settings.....	23
2.7 Form 3B+ Settings	24
2.8 BIO X settings.....	27
2.9 Settings applied for rheological analysis of hydrogel constructs.....	29
3.1 CELLINK Laminink 411 recommended settings.....	32
3.2 BIO X 405 nm crosslinking guide	33
3.3 Laminink UV crosslinking optimisation calculated from RF	34
3.4 Matrix stiffness in kPa for Laminink hydrogels at 200 % and 400 % RF increase.	34
3.5 UV settings used for all cell-laden Laminink hydrogel constructs	34
3.6 Matrix stiffness of Laminink hydrogels encapsulated in 2D PANC-1 cells. ..	35
3.7 Matrix stiffness of Laminink hydrogels encapsulated with microwell plate grown PANC-1 spheroids.	37
3.8 Collagen hydrogel construct mechanical testing results.....	38
4.1 BIO X parameters, modifications and considerations when bioprinting.....	42
1 Calculated surface areas within certain beam angles.	55
2 Scaled down version of table used to calculate mW/mm ²	57
3 Highlighted version of BIO X 405 nm crosslinking guide	58

Acknowledgements

I would like to express my appreciation to Prof. Hanne Hagland for the opportunity to combine the fields of biology, chemistry and 3D manufacturing into this project.

I am grateful to Gorana Drobac and Nofima for the generosity in providing training and granting access to their sensitive in-demand equipment.

My sincerest thanks to Nora Anise, Sheida Naderi and Marcus Roalsø in the provision of cultured cells for this project and to Yosef Adugna for providing access and invaluable experience to a multitude of 3D printer types.

Additionally, I would like to extend thanks to UiS for the opportunity to study a Master's degree – the experience has been excellent.

"A failure, no matter how dismal it may make the future seem, doesn't mean the end"

Franklin D. Roosevelt

Declaration

I, Scott George Paul, declare that this thesis titled, 'A Bioprinting Workflow for Live Cell Imaging and Mechanical Testing' and the work presented in it are my own. I confirm that:

- This work was done wholly or mainly while in candidature for a research degree at this University.
- Where any part of this thesis has previously been submitted for a degree or any other qualification at this University or any other institution, this has been clearly stated.
- Where I have consulted the published work of others, this is always clearly attributed.
- Where I have quoted from the work of others, the source is always given. With the exception of such quotations, this thesis is entirely my own work.
- I have acknowledged all main sources of help.
- Where the thesis is based on work done by myself jointly with others, I have made clear exactly what was done by others and what I have contributed myself.

Signed:



Date:

11th June 2023

Abbreviations

PDAC – Pancreatic ductal adenocarcinoma

DHR-2 – Discovery hybrid rheometer 20

UV – Ultraviolet

CAF – Cancer associated fibroblast

ECM – Extracellular matrix

2D – Two-dimensional

3D – Three-dimensional

MMP – Matrix metalloproteinases

CAD – Computer aided design

STL – Stereolithography

MRI – Magnetic resonance imaging

CT – Computerized tomography

FDM – Fused-deposition modelling

SLA – Stereolithography

LCD – Liquid crystal display

LFS – Low-force stereolithography

GelMA – Gelatin methacrylate

LAP - Lithium phenyl-2,4,6-trimethylbenzoylphosphinate

ATCC – American type culture collection

GLP-1 – Glucagon-like peptide 1

FGF-2 – Fibroblast growth factor-2

DMEM – Dulbecco's modified eagle's medium

PBS – Phosphate buffered saline

DMSO – Dimethyl sulfoxide

FBS – Fetal bovine serum

PPE – Personal protective equipment

UiS – University of Stavanger

RF – Radiant flux

LED – Light emitting diode

Chapter 1

Introduction

1.1 Pancreatic Cancer

Addressing the onset, progression and recurrence of cancer remains an enduring and central focus for biomedical researchers. Compounded by the diversity of cancer morphology, development, evolution, and treatment strategies, the all too well-known characteristic of this field is its scale. Researchers have been challenged by this incidental by-product of evolution to discover and form pathways to understand the complexities of cancer biology.

Pancreatic cancer continues to pose a particularly significant challenge. Pancreatic ductal adenocarcinoma (PDAC), the fully developed version of this cancer, is a leading cause of cancer mortality in the United States, with a 5-year survival rate near to 8 % [1]. In the European Union, predictions suggest that pancreatic cancer could surpass breast cancer as the third-leading cause of cancer-related deaths and an incidence rise of 10 % in the last decade in parts of the UK also suggests that this disease is on the rise [2].

The coarseness of PDAC originates in its complex, dense, and hypo-vascularized stroma which exhibits large associations of proliferating PDAC cancer cells, cancer-associated fibroblasts (CAFs), macrophages, immune cells, and excess extracellular matrix (ECM) proteins (figure 1.1) [1]. CAFs, which are integral to the development of the dense stroma, produce excess ECM proteins such as collagen and laminin [3]. The tumor mass that forms as a result of this effectively creates a barrier to chemotherapy exposure and other therapeutics [4]. Methods to penetrate this barrier to effect change on the cells is a central focus of pancreatic cancer research.

The absence of detection of this type of cancer in its early stages, combined with the fact that at present there are no definitive treatments truly demonstrates the importance for identifying potential markers able to detect the disease early enough in order for effective treatments such as resection via surgery to take place [5]. Only 15 – 20 % of diagnosed PDAC patients have resectable tumours at the time

of diagnosis and in addition PDAC itself exhibits a strong resistance to radiotherapeutic and chemotherapeutic treatments [1]. Curative therapies at present consist only of surgical removal of the tumor site, followed by adjuvant therapies [6].

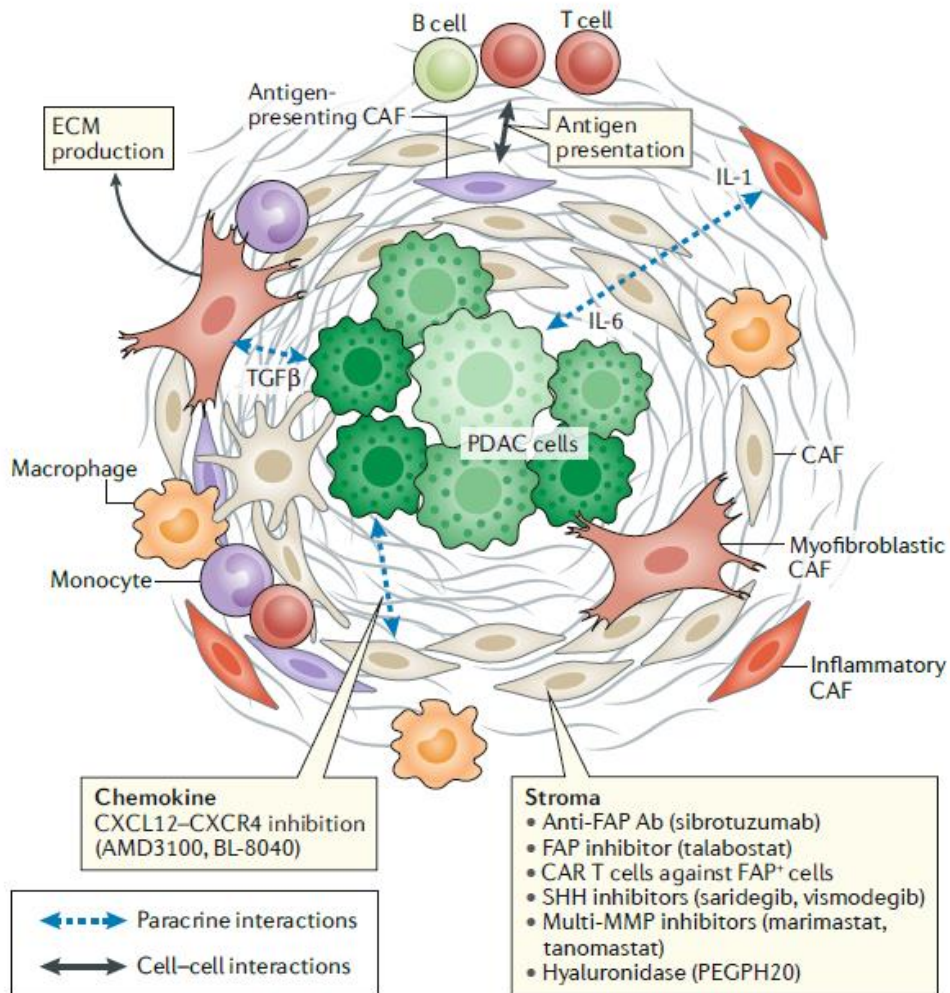


Figure 1.1. PDAC and the surrounding dense fibrotic tissue. Adapted in full from [3].

Combatting the challenge of pancreatic cancer and elucidating its biology to find new effective, experimental treatments thus represents an ongoing pursuit for researchers with many hurdles yet to be passed.

1.2 2D & 3D Cancer Models

As modern cancer research has developed, it is beginning to become clear that the reliance on the established standard two-dimensional (2D) surface cell culture methodology is inadequate to represent more complex *in vivo* tissues such as tumours (figure 1.2) [7]. It is being demonstrated that the 2D technique does not represent the intricacies of three-dimensional (3D) architecture found in cancer affected tissues [8]. Additionally, while 2D *in vitro* systems are easy to use and show effective responses to drugs and radiation they are not able to accurately represent many important aspects of *in vivo* 3D structures such as realistic cell-cell and cell-ECM interactions, structure, porosity, environmental gradients, presence of ECM proteins and vascularisation [9]. The lower dimensionality of the flatter 2D models can also cause inhomogeneities in the distribution of membrane-bound signalling molecules [10].

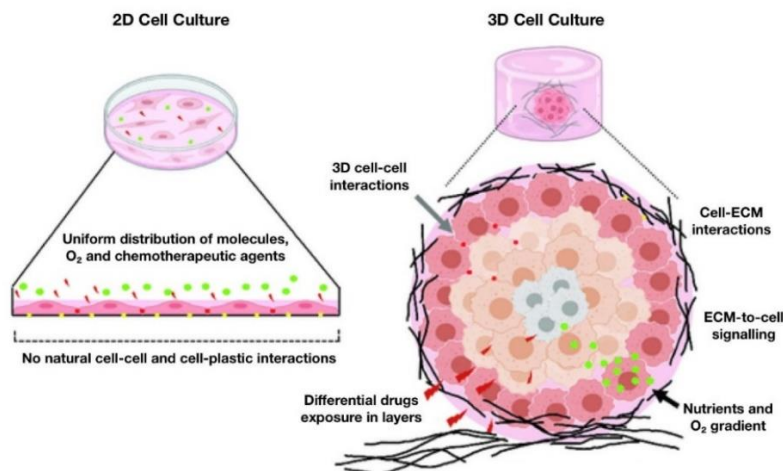


Figure 1.2. 2D and 3D cell culture differences. Adapted in full from [7].

As a result of the recognition of these limitations, a shift in interest from standard 2D culture models towards 3D *in vitro* cancer models is a process that is currently ongoing. Such 3D models are able to offer a more physiologically relevant approach towards the investigation of complex cancer biology [11]. The 3D spheroid, a cellular structure of cancer cells, is one such model that allows researchers to reproduce key features of *in vivo* tumours such as those already mentioned - the 3D architecture, cell-cell interactions and environmental gradients [4]. Worth noting are some important differences in cellular behaviour between 2D and 3D environments. ECM degrading matrix metalloproteinases (MMPs) expression is essential for the growth of capillaries in 3D whilst in 2D their expression can be absent [12]. The effect of matrix stiffness and cell adhesion ligand concentrations in two or three-dimensions has also been shown to influence endothelial cell migration and network branching [12].

With the increased interest towards 3D cancer culture models, recent advances combining biology and aspects of engineering have moved towards the development of *in vitro* pancreatic organ-on-a-chip devices capable of simulating aspects of active pancreatic islets [6]. These models have been shown to be highly sensitive to drug treatments, thus arming researchers with a tool to discover and perform studies into the therapeutic efficacy of explorative pancreatic cancer treatments. These devices, whilst capable of being designed around spheroids, have found use by being represented by another, improved model - the 3D organoid. These complex 3D cellular structures are able to mimic the architecture and function of native organs and tissues. They have also demonstrated their use as a valuable preclinical screening platform for their unique ability to mimicry [13]. Organ-on-a-chip devices now present an opportunity to study cellular/physical barriers, shear stress modulation events, physiological fluid flow and nutrient feed dynamics [4]. The end result of this technology may likely enable the large-scale elucidation of many of the aspects native features occurring in *in vivo* tumours that we do not currently understand today. Thus, the progression from 2D to 3D research represents an interesting phase in the continued progress of cancer research, by providing more advanced, personalised, and realistic models to researchers. A change that inevitably could bring positive developments in therapeutic treatments to this vast area of research.

1.3 Bioprinting in Cancer Research

Bioprinting, the technology that combines the principles of engineering, biology, chemistry, medicine and biomaterials science into a format assessable to researchers of many backgrounds and expertise, can offer solutions to issues in cancer research. A recent shift towards this accessible technology has resulted in the arrival of commercial 3D bioprinters, of which the BIO X 3D bioprinter from CELLINK, Sweden, is one such example (figure 1.3) [14].



Figure 1.3. The BIO X 3D Bioprinter from CELLINK. Adapted in full from [14].

Bioprinting provides a method to simulate the diversity of tissue-specific architecture through the specific deposition of cell-laden bioink in a preordained path. This has effectively advanced the system by which tissue modelling can be achieved [6]. The innovative nature of this technology can permit the fabrication of *in vitro* 3D cancer culture models in a single step, allowing for the rapid localization of multiple cells within specific biomaterials in order to try to emulate the *in vivo*-like microenvironment of native tissues [6]. It is a technology that by design allows precise, reproducible cell-positioning that can enable the manufacture of functional pancreatic tissue models [6]. In addition, multi-material designs are also possible [15].

In the context of cancer research, bioprinting has found many applications with the ability to facilitate the creation of tumor microenvironments, thus improving the modelling of cancer types and enhanced drug screening. Patient-personalised 3D tumor masses developed using bioprinting could in theory mirror the patient's own tumor tissue at the detection stage [13]. Such *in vitro* models may provide invaluable when considering the nature of pancreatic cancer. The rapid production of models with biomimetic tumor constructs that have reproducible geometry, tuneable mechanical properties and biological components, alongside comparable functional complexity offers a method for improving patient-specific treatment strategies [4]. Positive aspects of the technology cannot be stated without also mentioning negative ones. Despite impressive advancements in the quality of commercial devices, significant challenges remain. Long-term viability of bioprinted structures is one such issue. Another is the ability to maintain the sterility of constructs when printing. Achieving the desired functionality in order to reach a point of mimicry where the *in vitro* model matches that of the *in vivo* physiological environment is clearly one of the largest hurdles types of research into this field presents. With this said, the journey towards harnessing functional bioprinted structures with respect to cancer biology is promising, and it does offer the possibility to improve the understanding of cancer and related treatment strategies.

1.4 Bioprinting Principles

Understanding the process of bioprinting begins with knowledge about computer-aided design (CAD) software. The purpose of which, simply put, is to enable users to create 3D digital models. Examples of CAD software include:

- AutoCAD, subscription-based service used by professionals.
- Fusion 360, free to students.
- Blender, free and open-source.

All of these are capable of producing stereolithography (STL) files, which act to describe surface geometry and produce a mesh by which a 3D object can be represented digitally. STL files are then transferred over to a second piece software known as a Slicer. These are used to create a G-code files, which act as a guide for the bioprinter. Slicers can be device specific, as certain manufacturers only allow their slicing software to be used. However, since 3D bioprinters have similar hardware designs to 3D printers, a slicer for a 3D printer can also be used for a 3D bioprinter. Models can be based on medical imaging data such as Magnetic resonance imaging (MRI) or computerized tomography (CT) scans, thus allowing accurate representations of the internal components of the human anatomy to be readily accepted by bioprinters. A number of 3D bioprinting techniques exist to replicate the architecture of native tissues [13]. The two considered here are extrusion and light-based methodologies (figure 1.4) [16].

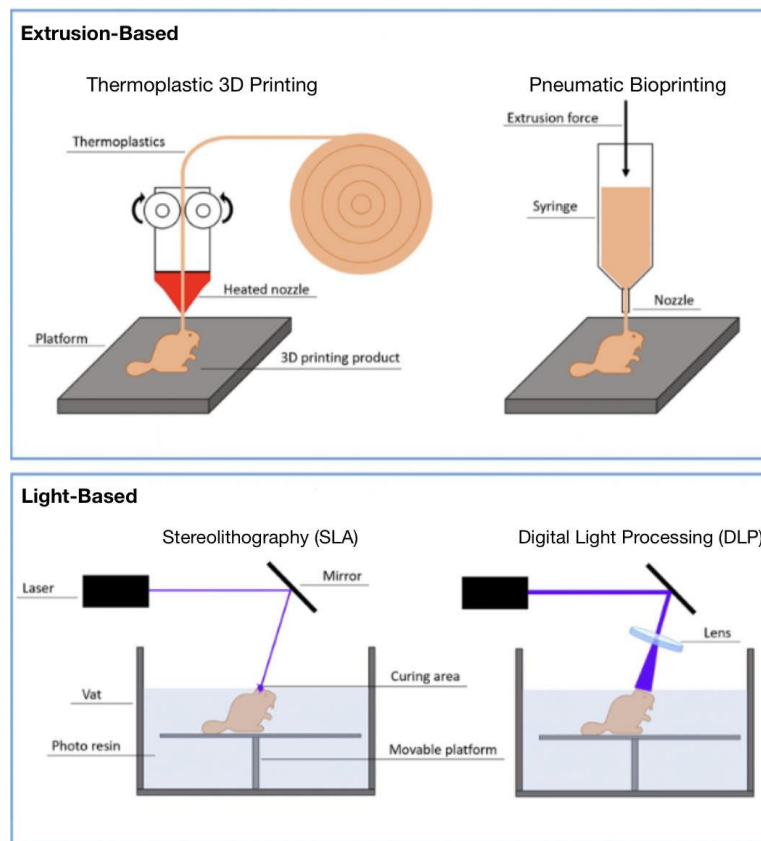


Figure 1.4. Extrusion- and light-based methods for 3D printing. Adapted in part from [16].

Extrusion based: A method in which the bioink / cell-laden hydrogel is loaded into a syringe and then extruded out of a nozzle by either air (pneumatic) or mechanical (screw / piston) forces. The method for bioink deposition follows the same principles as fused-deposition modelling (FDM) processes in 3D printing [13]. The toolhead follows the path defined by the G-code and once a layer has been set down, pauses, increases the z-axis direction height by a specific distance, then proceeds on with the second layer. The process continues until the specific design determined by the STL file is completed. This method is largely used, it gives the

user a high degree of freedom with respect to bioink material choice and as such is open to bioinks with high cell densities and those of high viscosity. The range of nozzle types and size available are highly custom, and thus structures of relatively high accuracy can be achieved. However, the shear-strain mechanical forces imposed on the cells during the extrusion, depending on the nozzle size and the pressure imposed on the bioink in order for extrusion to proceed, may impose such an external pressure on the external cellular environment that disruption to cellular structures occurs resulting in low survivability for example, organised and delicate 3D structures such as spheroid and organoids. Such is the technology used by the BIO X 3D bioprinter from CELLINK, Sweden.

Light based: This approach uses light of a specific wavelengths to polymerise photoactive bioink / cell-laden hydrogels [13]. It can be separated into different versions based on the how the light is transferred to the photoactive bioink. One method is stereolithography (SLA). In SLA printing, by placing a liquid crystal display (LCD) screen between a UV light source and the biomaterial whilst simultaneously controlling which pixels on the screen allow the passage of light through the screen, a controlled region of biomaterial on the surface of a rigid tank is exposed to UV light, which then reacts and solidifies. Thus, instead of a layer having to be deposited over a period of a few seconds, in this technique an entire layer of the bioink can be exposed at once, such a layer-by-layer process decreases the total bioprinting time [17]. Resolution depends on the density of pixels on the LCD screen. A cost of the increased speed is the potential significant exposure of a particularly damaging wavelength of light to cells, which may decrease cell survivability. Another version of this technology, with minor changes, is known as low-force stereolithography (LFS) technology. LFS 3D printing, instead of a rigid tank for UV exposure, uses a flexible one to improve characteristics of the final print including. LFS is used by the Formlabs 3B+. Another version is DLP, where instead of light being delivered through pixels, the light controlled by mirrors is used to project the image of an entire layer simultaneously. This is used in the Lumen X+ 3D printer from CELLINK.

1.5 Hydrogel Networks

Hydrogel networks are the name given to three-dimensional structures formed via the crosslinking of monomers that functional as the base material for bioprinters [4]. They are also known as hydrogels, or bioinks. Crosslinking results in an interconnected networks that have the ability to retain significant volumes of water, hence the name hydrogels. The method by which crosslinking is initiated may be as a result of photo-, enzymatic, thermal and ionic processes with each methods influencing a unique effect on hydrogel properties such as matrix stiffness, porosity and degradation rate [13]. Thus, hydrogel networks are highly

customizable structures. Their versatility allows for a high number of possible combinations of cells in order to form final 3D constructs for biomedical research purposes. Hydrogels therefore have found use in fields such as drug delivery and tissue engineering [18]. Material selection and network design is an increasing field of research in modern times. In order to assess their performance for bioprinting, each hydrogel has a defined printability, also termed printability window, in which a balance is struck between their cell compatibility and mechanical properties [19]. Understanding hydrogel printability allows bioprinting to proceed, ensuring suitable resolution for printed structures and the desired shape fidelity post-printing [13].

Hydrogel printability depends on a number of mechanical properties such as viscosity, matrix stiffness and the nature of the gelation kinetics [13]. All are important in maintaining a constant printing process, whether it is a constant flow rate in extrusion-based methods or a homogeneous UV-curing in light-based methods [17]. Depending on the method chosen for printing, it is important that these base biomaterials avoid low and high-viscosities. Low viscosity results in the materials taking on the nature of liquids, which would make extrusion challenging due to controlling the low pressures required. In addition, liquids would simply leak out from a bioprinter in extrusion-based methods. High viscosity results in such high pressures required for extrusion that cells going through a nozzle experience what is known as shearing, a process by which cells are crushed under the combined effect of high pressure and confined spacing that occurs inside the small nozzle diameters used in extrusion-based methods [20].

An ideal hydrogel resembles the ECM of a chosen biological tissue, such as the pancreatic islets within the pancreas. The likeness to natural ECM makes these materials ideal environments that can promote *in vitro* native cellular growth and function similar to that observed *in vivo* [1]. Thus, as ECM mimics, these materials are designed to function as 3D scaffolds that can promote cell adhesion, proliferation, differentiation and growth. The combination of appropriate cell-adhesion cues are significant here, with the incorporation of recognition sequences in the hydrogel network proving useful in providing cells with the environments they need to have high, long-term viability. Such cues are particularly important in the adjustment of the recently encapsulated cells to their new hydrogel network-based environment. In order to maintain and promote cell viability, hydrogels are commonly exposed to the same media as standard 2D model systems. The potential for the addition of other molecules, can also be important in establishing cell growth and tissue formation in these environments. The variations of networks possible with changes to or additional functionalization possible also present other means to achieve a stable *in vitro* 3D environment. Tailoring the principles underlying aspects of hydrogel network formation are thus an intense area of study. The following examples of hydrogels have shown promise in the pursuit of a bioprintable material that can be used to achieve an optimal hydrogel construct for a wide-range of tissue types.

1.5.1 Matrigel

Matrigel, a marketed hydrogel material formulated from the secretions of Engelbreth-Holm-Swarm mouse sarcoma cells is widely used in biomedical research today [21]. Primarily composed of laminin, collagen IV and entactin, this material is known to mimic native ECM effectively. Also contained within its network are a multitude of growth factors, matrix proteins and attachment sites for cells. This unique composition however does represent a significant limitation of the material - often its exact composition is unknown. The method for its production introduces an inherent variability between production batches and as such it makes it challenging to achieve experimental consistency [21, 22]. Proteomic analysis of Matrigel samples has shown that it can contain more than 1800 unique proteins [21]. This complexity is not ideal when trying to define and identify specific factors governing cellular processes. Matrigel useability in bioprinting is possible as it undergoes temperature-mediated gelation above 4°C, albeit it would be a challenging process requiring meticulous optimisation and time-orientated steps. Access to the quantities required to create a bioprinting protocol for this material is generally not possible due to the associated cost of this material. It does however represent an effective ECM mimic for which other hydrogel materials can aspire to.

1.5.2 Laminink 411

Laminink 411, the hydrogel of focus in this study alongside collagen, is a marketed material from CELLINK consisting of porcine gelatin functionalized with methacrylate groups (GelMA, approximately 45 – 55% degree of methylation), xanthan gum, alginate and several laminins (figure 1.5) [23]. It has been developed with xanthan gum and alginate in order to enhance its printability and ease-of-use. Inclusion of laminins within the hydrogel network is done to promote mimicry of native microenvironments. The presence of alginate allows ionic crosslinking with a CaCl_2 solution, while a photoinitiator (Lithium phenyl-2,4,6-trimethylbenzoylphosphine, LAP) is also present to allow UV crosslinking at 405 nm.



Figure 1.5. A 3 mL Laminink 411 cartridge and CaCl_2 crosslinking solution produced by CELLINK. Adapted in full from [23].

1.5.3 Alginate

Alginate, a naturally derived polysaccharide which originates in the cell walls of brown algae, is another important material being used in modern biofabrication processes. It has a structure consisting of β -D-mannuronic acid and α -L-guluronic acid residues and its properties allow it to demonstrate good biocompatibility and hydrogel network formation via an ionic crosslinking of cations such as calcium. As a biomaterial, the ionic gelation mechanism allows for mild crosslinking in the presence of cells, a characteristic that is essential in preserving cell survival. It has diverse functionalisation possibilities and viscosity adjustments through concentration changes facilitate its adaptability to different bioprinting techniques [19].

One of the earliest uses of this material in 3D bioprinting involved the extrusion of a cell-laden alginate solution that was pre-crosslinked through use of a calcium chloride (CaCl_2) solution. Extrusion of the hydrogel into a container filled with CaCl_2 solution allowed a semi-crosslinked material to become fully-crosslinked in a mild matter [19].

A disadvantage of alginate as a biomaterial however is its inherent lack of cell-adhesive attachment sites, known as motifs. These sites are important for cells to identify their environment, and in order them to function as they normally would *in vivo*, such *in vitro* models require the presence of important motifs. Functionalisation of alginates is almost always required due to this. In addition, the diffusion of cations out of the gels can lead to a loss of structural integrity since such cations are essential in maintaining a crosslinked hydrogel. However, alginates have been shown to demonstrate the ability to maintain their mechanical stability for prolonged periods when incubated in cell culture media for up to 3 weeks [24]. In addition to this, their ability for as a suitable cell storage material has been shown when a study showed that alginate-encapsulated human adipose-derived stems cells were able to survive storage at 15 C for one week [20].

Due to their versatile nature and that this material is potentially capable of encapsulating different cell types, alginates are subject to increased interest a bioprintable material.

1.5.4 Collagen

Collagen hydrogels have piqued interest as a functional bioprinting material due to collagens abundance in various tissues throughout the body. It is the major ECM components in the solid tumor tissue of pancreatic islets and their periphery [6]. Collagen molecules are recognised for their ability to provide to high biocompatibility and appropriate cell-adhesion sites that promote cells to adhere, proliferate and differentiate [21]. In addition to the favourable structural qualities

of collagen, this molecule also acts as a signalling molecule that can instigate a number of interactions between cells such as migration processes and morphogenesis events [25].

These properties, along with its ability to demonstrate mechanical flexibility and the capacity to form functionalised hydrogel networks show its potential as a hydrogel material. By already containing certain motifs required by cells, less functionalisation is required in order to promote cellular attachment. For potential use *in vivo*, the fact that this material is inherently biodegradable and allows the formation of new tissue over artificial collagen hydrogel networks is favourable if they were ever to be used within the body [26].

As a bioprinting material, it has already established use in this field. A notable example is in skin tissue engineering, where bioprinted collagen constructs have demonstrated the ability to replicate the native ECM of skin dermis, promoting fibroblast proliferation and the formation of a collagenous matrix [27]. It is hoped such materials will one day see use in the personalised treatment of burn patients.

In relation to pancreatic cancer studies, PANC-1 cells encapsulated in collagen gels have been shown to be able to remodel their local environment in order to transition in a ductal phenotype which is important for studying the disease [22]. Another study has shown the successful use of hydrogel networks containing collagen IV, fibronectin and laminin for the culture of pancreatic mouse islets [28]. In particular, the presence of collagen IV has been found to promote the viability and survival of pancreatic islets [6]. With the innate biocompatibility and wide-ranging uses, collagen serves as an important base material in 3D bioprinting.

1.6 Live Cell Imaging & Confocal Microscopy

The ability to perform live cell imaging is an invaluable technique to allow for the real-time observation of cellular dynamics, signalling and behaviour, giving an understanding of processes within *in vivo* or *in vitro* environments. Confocal microscopy, a branch of microscopy developed in the 1950s, allows for the production of 3D information on a microscope via the creation of optical sections when imaging [29].

In difference to standard microscopes, in which all emitted light from a fluorescent sample is collected, confocal microscopes employ a pinhole or spatial filter in the confocal plane of the lens. This design separates in- and out-of-focus light, allowing only in-focus light to reach the detector. The in-focus light produces high-resolution images and subsequently by taking in-focus images at different heights through a 3D sample, known as optical sectioning, a 3D visualisation of a sample can be constructed [29]. Due to the 3D nature of hydrogels, confocal microscopy presents an ideal technique for their study.

Imaging of hydrogels seeks to determine and verify both the cell survival post-printing and the spatial distribution of cells. Repeated imaging over time can allow for the identification of any potential cellular interactions, offering an ability to study matrix remodelling within hydrogel networks.

Challenges in this method include the potential for phototoxicity, resulting from an either inappropriate stain choice or staining methods, or photobleaching in which intense light exposure to cells leads to death. The versatility of stains available to be used for hydrogel networks are vast, with a wide range of fluorophores available to study an equally wide range of cellular components. Confocal microscopy is undoubtedly an essential tool in assessing the useability of bioprinted constructs.

1.7 Mechanical Testing & Rheology

Understanding the mechanical properties of any bioprinted structures is essential to create constructs with physiological relevance. Pancreatic cancer tumor tissue has a reported range of between 2 and 6 kPa, and as such any *in vitro* 3D model system would need to mimic this [27, 30, 31]. Replicating mechanical stiffness in 3D models applies to all tissues of interest.

In order to perform such testing, texture analysers and rheology devices can be used. Texture analysers operate by applying a known force to a sample and measuring the response, thereby providing information about the materials texture, measurements of matrix stiffness in kPa, a defined mechanical property of hydrogels, can be obtained by this method [32].

Another method to determine matrix stiffness that this study focuses on is the use of rheometers, devices that study the flow and deformation of matter. Rheology provides insight into a materials viscosity, elasticity and viscoelasticity. Viscosity being the resistance of a material to flow under an applied force, elasticity representing a materials ability to revert to an original state post-deformation and viscoelasticity, a characteristic that describes a material to display both liquid and solid properties depending on certain conditions [20]. The mechanical properties are influenced by hydrogel network composition, and thus determination of stiffness with use of rheometers can be used for assessing the successful, reproducible production of bioprinted constructs and for optimisation attempts for hydrogel network prototyping. Challenges of the mechanical testing are many, and it is known that gels are a particularly challenging material for study primarily due to sample preparation and handling.

1.8 Aims and Objectives

The main aim of the project was the development of a repeatable, reproducible, and efficient bioprinting workflow that in the long term could establish a resilient method to replicate the stiffness and composition in found in *in vivo* organ tissues.

Additional aims and objectives include:

- To allow the real-time observation of cell viability within bioprinted constructs, whilst simultaneously enabling an accurate assessment of mechanical properties.
- To show that inclusion of UV, ionic and temperature-mediated crosslinking processes enable the researcher a means of mimicking native tissue stiffness ranges observed across both normal and tumor-bearing tissues.
- To provide a method by which bioink formulations can be optimised for enhanced printability, cell viability and mechanical properties.
- To give a method by which the long-term biological performance of hydrogel constructs can be assessed.
- To show intent towards more effective tools to study pancreatic cancer in order to contribute towards a model that can be dedicated towards more effective therapeutics for personalized medicine.
- The adjustable nature of the protocol aims to show relevance towards other tissue types and diseases.

Ultimately, the author wishes to demonstrate that the bioprinting workflow outlined demonstrates a means by which an end goal towards the creation of a functionally viable *in vitro* 3D cancer culture model could be achieved.

Chapter 2

Materials and Methods

2.1 Materials

2.1.1 Cell Lines

The PANC-1 cell line was the only cell line used in this study. The details for this cell line including its American Type Culture Collection (ATCC) number are stated below in table 2.1.

Table 2.1. PANC-1 cell culture line ATCC No. and details.

<i>Cell Line</i>	<i>ATCC No.</i>	<i>Tissue</i>	<i>Disease</i>	<i>Source</i>	<i>Morphology</i>	<i>Growth Properties</i>
PANC-1	CRL-1469	Pancreas /Duct	Epithelioid carcinoma	Human, 56-year male	Epithelial	Adherent

PANC-1 cells are an established cell line that provides a good representation of pancreatic tumor tissue. Their high proliferation in standard culture conditions makes them well suited to use in a broad range of experiments.

Lineage reprogramming into insulin-secreting cell clusters can take place on these cells with the use of soluble cues such as glucagon-like peptide 1 (GLP-1), fibroblast growth factor-2 (FGF2) and stem cell factor [22]. The small multicellular clusters that form have been studied in a number of hydrogel studies [1, 15, 18].

2.1.2 Reagents

A list of reagents, manufacturers, reference numbers and associated purpose in the work performed throughout the study is presented below in table 2.2.

Table 2.2. Reagents, associated manufacturer, reference numbers and purpose.

<i>Reagent</i>	<i>Manufacturer</i>	<i>Reference No.</i>	<i>Purpose</i>
Dulbecco's Modified Eagle's Medium (DMEM, 500 mL)	Corning	17-207-CV	Cell culture & collagen preparation
DMEM Powder (8.3 g/L)	Corning	90-113-PBR	Cell culture & collagen preparation
L-Glutamine (200 mM)	Corning	25-005-CI	Cell culture & collagen preparation
D-(+)-Glucose (1 M)	Sigma-Aldrich	G7021	Cell culture & collagen preparation
Penicillin-streptomycin 100X solution	HyClone	SV30010	Cell culture & collagen preparation
Sodium chloride	Sigma-Aldrich	S5886	Cell culture & collagen preparation
Sodium bicarbonate	Sigma-Aldrich	71627	Cell culture & collagen preparation
Phosphate buffered saline (PBS, tablets)	ThermoFisher	003002	Cell culture & collagen preparation
Sodium hydroxide (NaOH) pellets	Avantor	7097	Cell culture & collagen preparation
α -Chymotrypsin (trypsin)	Sigma-Aldrich	C3142	Cell preparation
Fetal bovine serum (FBS) (10 %)	Biowest	1810-500	Cell culture
Hydrochloric acid (HCl, 37 %)	Fisher Chemical	H/1200	Cell culture
TeloCol-10 (10.2 mg/mL)	Biomatrix	5226	Collagen preparation
HEPES (≥ 99.5 %)	Sigma-Aldrich	H3375	Collagen preparation
GelXA Laminink 411	CELLINK	IK3X21230303	Bioprinting
Crosslinking agent (CaCl ₂ , 50 mM)	CELLINK	CL1010006001	Bioprinting
MitoTracker Deep Red FM	Invitrogen	M22426	Live cell staining
Calcein, AM	ThermoFisher	C3099	Live cell staining
Dimethylsulfoxide (DMSO)	Life Technologies	L34951	Live cell staining
Muse count & viability kit	Luminex	MCH100102	Cell viability determination
PLA Filament (1.75 mm, 2 kg)	Prima Creator	Not found	3D printing
Biomed White Resin (1 L)	Formlabs	RS-F2-BMWH-01	3D printing
2-Propanol (≥ 99.0 %)	VWR Chemicals	20839.366	3D resin part washing

2.1.3 Prepared Solutions

2.1.3.1 Complete Cell Media (cDMEM)

For the standard 2D culture of PANC-1 cells in cell culture flasks a 500 mL supplemented version of DMEM was made.

- 500 mL DMEM solution
- 50 mL FBS
- 5 mL Penicillin-streptomycin X100 solution
- 5 mL L-Glutamine (200 mM)

All items were transferred to a sterile fume cabinet. The FBS, penicillin-streptomycin and L-glutamine solutions were added sequentially to the DMEM using the appropriately sized pipette (5 mL, 25 mL) and a pipette controller. The final solution was mixed via pipette-induced mixing and stored at 4 °C. The complete cell media was warmed in a water bath set to 37 °C prior to use.

2.1.3.2 Imaging Solution

In order to avoid additional fluorescence during the confocal imaging in the cell culture media required by hydrogel constructs, it was decided that an 'imaging solution' be prepared. This was performed according to a previous study [33].

- 0.414 g DMEM powder (8.3 g/L)
- 0.09 g Sodium chloride
- 0.185 g Sodium bicarbonate
- 1250 µL Glucose (1 M)
- 500 µL L-Glutamine (200 mM)
- 5000 µL FBS (10 %)
- 500 µL Penicillin-streptomycin 100X solution
- 3.7 % HCl
- Milli-Q water

DMEM powder, sodium chloride and sodium bicarbonate were weighed and transferred to a sterile fume cabinet. To a 50 mL falcon tube, 25 mL Milli-Q water was added. DMEM, sodium chloride and sodium bicarbonate were then sequentially added to the falcon tube and mixed until fully dissolved. The required volumes of glucose, L-glutamine, FBS, and penicillin-streptomycin were added using a micropipette. Milli-Q water was added to the falcon tube to bring the total volume to approximately 48 mL. At this point, using a micropipette, 200 µL

aliquots of 3.7 % HCl was added using a micropipette. After each aliquot, the pH of the solution was measured using Litmus paper. Continued addition of HCl aliquots were added, as needed, until it was determined that the solution was at pH 7.4. The 50 mL falcon tube was labelled and stored at 4 °C. The imaging solution was warmed in a water bath set to 37 °C prior to use.

2.1.3.3 HCl (3.7 %)

A 10X dilution of 37 % HCl was required in order to adjust the pH of the imaging solution.

- Hydrochloric acid (37 %)
- Milli-Q water

To a 15 mL falcon tube, 9 mL of Milli-Q water was added using a 10 mL pipette. Using a pipette, 100 µL hydrochloric acid (37 %) was added. The final solution was stored at room temperature and used for pH adjustments when required.

2.1.3.4 HEPES (100 mM)

A diluted HEPES solution was required and prepared in order to buffer the collagen solution during collagen gel preparation. A two-step synthesis was performed. This was performed according to a previous study [33].

Step 1: Preparation of 1 M HEPES

- 2.38 g HEPES powder
- 10 mL Milli-Q water

To a 15 mL falcon tube, 10 mL of Milli-Q water was added using a 10 mL pipette. HEPES powder (2.38 g) was weighed into a weighing boat and transferred into the falcon tube. The tube was capped and inverted several times until the powder was dissolved.

Step 2: Preparation of 100 mM HEPES

- 1 mL HEPES 1 M solution
- 4 mL 5X PBS
- 5 mL Milli-Q water

A total of 5 PBS tablets were dissolved in 100 mL Milli-Q water to make a 5X PBS solution. In a 15 mL falcon tube, using a 5 mL pipette, the required volumes of HEPES, X5 PBs and Milli-Q water were combined and 1 mL aliquots were

prepared into 1.5 mL Eppendorf tubes. The final 100 mM HEPES solutions were then stored at -20 °C.

2.1.3.5 NaOH (5N and 0.5N)

A two-step synthesis was performed for these solutions in a similar manner to the 100 mM HEPES solution.

Step 1: Preparation of 5N NaOH

- 40 g Sodium hydroxide pellets
- 100 mL Milli-Q water

Sodium hydroxide pellets were weighed and added to a beaker containing a magnetic stirrer bar and 100 mL Milli-Q water. The solution was heated on a hot plate slightly and stirrer magnetically until the pellets were fully dissolved. The solution was then left to return to room temperature before use in step 2.

Step 2: Preparation of 0.5N NaOH

- 1 mL 5N NaOH
- 9 mL Milli-Q water

Dilution of 1 mL 5N NaOH solution with 9 mL Milli-Q water in a 15 mL falcon tube was performed to form the final 0.5N NaOH solution. The final solution was stored at room temperature and used for pH adjustments when required.

2.1.3.6 Collagen Gel (3 mg/mL)

Prior to the encapsulation of cells, 3 mL aliquots of collagen gel were prepared and placed into 3 mL syringes. This was performed according to a previous study [33]. The procedure was performed in a cold room (approximately 6 °C) and all solutions were placed on ice, in order to keep the collagen at a low temperature so that potential for temperature-mediated gelation was minimised. First, the desired final collagen concentration (3 mg/mL) and the required collagen volume was calculated. To an ice-cooled falcon tube, collagen (10.2 mg/mL) was added and diluted with X1 PBS. The solution was then buffered with 1:1 HEPES (100 mM). Using cold 5N or 0.5N, the pH was adjusted to 7.4 with indicator strips and gently mixed to form the final collagen solution. It was important to minimise air bubbles during mixing. A back-and-forth motion with the tube in-hand was used to remove any air bubbles present. The final collagen solution was then transferred to a 3 mL syringe and stored at 4 °C for further use.

2.1.4 Consumables

A list of consumables used throughout the work performed is presented below in table 2.3.

Table 2.3. A list of consumables, associated manufacturer and purpose.

<i>Consumable</i>	<i>Manufacturer</i>	<i>Reference No.</i>	<i>Purpose</i>
Cell Culture Flasks	Falcon, Corning	-	Cell culture
96-Well Microplate	Greiner Bio-One	650101	Spheroid culture
μ -Dish 35 mm	Ibidi	81156	Hydrogel preparation, imaging, mechanical testing
Syringes (1 mL, 3 mL, 5 mL)	BD Plastipak	-	Cell encapsulation
Female / Female Luer Lock Adapter	CELLINK	OH000000010	Cell encapsulation
BIO X Cartridges (3 mL)	CELLINK	CSC010311101	Bioprinting
22G Nozzle	CELLINK	NZ3270005001	Bioprinting
Micropipette Tips	VWR	-	Solution handling
Acrodisk Syringe Filter (0.2 μ m)	ThermoFisher	17124381	Solution sterilisation
pH Indicator Paper	Merck Millipore	WHA10362000	pH adjustment

2.1.5 Instruments

A list of instruments used throughout the study is presented below in table 2.4.

Table 2.4. A list of instruments, associated manufacturer and purpose.

<i>Instrument</i>	<i>Manufacturer</i>	<i>Purpose</i>
Finnpipettes®	ThermoFisher	Cell & solution handling
PipetteBoy®	Integra Biosciences	Cell & solution handling
Centrifuge (Model 2800)	Kubota	Cell & solution centrifuging
CO ₂ Incubator (MCO-18AIC)	Sanyo	Cell incubation
Incubator (INCU-Line IL10)	VWR	Cell incubation
Water Bath (T100)	Grant Instruments	Cell & solution heating
Cell Analyser	Muse	Cell analysis
BIO X 3D Bioprinter	CELLINK	Bioprinting
Confocal Microscope (TCS SP8 SMD)	Leica Microsystems	Imaging
Rheometer (Discovery HR-2)	TA Instruments	Mechanical testing
FDM 3D Printer (Pro2 Plus)	Raise3D	3D printing
SLA 3D Printer (Form 3B+)	Formlabs	3D printing
Wash and Cure Station	Formlabs	3D printing

2.2 Methods

Aseptic conditions and techniques were maintained for all cell handling procedures. The work was performed in a sterile environment with the use of appropriate personal protective equipment (PPE). The nitrile-gloves worn were sterilised with 70 % ethanol before use. Fume cabinets pre-sterilised by UV were sterilised with 70 % ethanol before use. All materials and solution containers before placement in the fume cabinet were also sterilised with 70 % ethanol.

2.2.1 2D Cell Preparation

PANC-1 cells to be used in the study first had to be resuscitated from liquid-nitrogen storage. A liquid-nitrogen cooled Eppendorf tube containing PANC-1 cells was removed from storage and brought up to room temperature. The contents were transferred to a standard cell culture flask and 10 mL complete DMEM was added. Three times a week, media exchanges were performed to continually supply the cells with a fresh source of media. Spent media was removed with an aspiration pipette (2 mL) and replaced with pre-warmed cDMEM (10 mL).

In order to prepare cells for encapsulation with hydrogels the following steps were performed:

1. Remove media from cell culture flask using an aspiration pipette and wash with 5 mL X1 PBS. Remove PBS.
2. Add 1 mL trypsin to cell culture flask. Wait for cell detachment (≈ 3 min).
3. Add 9 mL cDMEM. Using a pipette, vortex cells until homogenous and transfer 9.5 mL cell solution to 15 mL falcon tube.
4. Place remaining 0.5 mL into a 1.5 mL Eppendorf tube. Add muse cell & viability reagent, wait for reaction to proceed (5 min) and analyse on Muse Cell Analyser to determine '% cell viability' and 'viable cells / mL'.
5. Use 'viable cells / mL' to calculate cell solution volume required.
6. From the 15 mL falcon tube, transfer required solution to an empty falcon or Eppendorf tube. Perform centrifugation and remove supernatant.
7. Resuspend cells with required imaging solution or cDMEM (200 μ L) to prepare the final cell solution ready for encapsulation within a hydrogel.

2.2.2 Hanging Drop 3D Spheroid Preparation

This method was not performed by the author but instead by a fellow University of Stavanger (UiS) student. It is included as to provide a complete account of the methods used in this study. A two-step synthesis was performed to prepare hanging drops for encapsulation:

Step 1. Cell Solution Preparation

1. Calculate the required number of cells to achieve considering 10,000 cells per spheroid in 40 μL of cDMEM. Include extra cell suspension (10 %) to account for any pipetting losses.
2. Mix the cell suspension by pipette induced vortexing to ensure even distribution of cells.

Step 2: Hanging Drop Preparation

1. Using a 100 μL micropipette, dispense a 40 μL droplet of the cell suspension onto the inverted lid of a sterile culture dish. Repeat for the required number hanging drops, ensuring appropriate spacing between droplets to mitigate against potential merging of drops.
2. With a rapid and careful motion, invert the culture dish lid and place into the bottom section of the sterile culture dish containing sterile X1 PBS.
3. Incubate (37°C, 5% CO₂) until ready for encapsulation (\approx 7 – 10 days).

2.2.3 Microwell 3D Spheroid Preparation

This method was not performed by the author but instead by a fellow UiS student. It is included as to provide a complete account of the methods used in this study. The following steps were performed to prepare microwell grown PANC-1 spheroids.

1. In the same manner as the 2D cell preparation, perform steps 1 – 5 to produce a 15 ml falcon tube containing a cell solution of PANC-1 cells.
2. Using the '% cell viability' and 'viable cells / mL' obtained from the Muse Cell Analyser, calculate the volume required to seed 5,000 cells per 50 μL in individual wells of a 96-microwell plate. Add 200 μL of X1 PBS to unused wells to prevent evaporation.
3. Incubate (37°C, 5% CO₂) until ready for encapsulation (\approx 7 – 10 days).

2.2.4 3D Designs and Slicer Settings

A summary of the 3D design methods to produce G-codes for bioprinting and 3D printing are detailed below. The CAD software Blender was used to create all STL files. Each blender design begins with the creation of a new 'general' file, with the units set to mm and the scale to 0.001 – this allows appropriate scaling when printing. Multiple slicing software was used as this software is generally printer-specific. Slicer settings were adjusted as required.

2.2.4.1 Construct for Cell Viability and Viscoelasticity Testing

A 20 mm x 20 mm x 1.5 mm cylinder was designed in Blender for the purpose for performing the cell viability and viscoelastic mechanical testing. The discs shape and size were chosen to suit available hardware, consumables and material specific parameters. For the DHR-2, a 20 mm stainless steel crosshatched (named in TRIOS as XHATCH) peltier plate was available for rheological testing. Coincidentally, this size also matched the lower surface area of an Ibidi 35 mm μ -Dish microscope slide, and thus bioprinted constructs could be imaged and mechanically tested. A degree of sterility could be maintained in these dishes, and additionally media exchanges and exposure of cells to stains could be performed.

A CELLINK document stated that that every 4th layer required one crosslinking event with a UV module [34]. A construct with a z-height of 1.5 mm was therefore chosen as it would result in the formation of 4 bioprinted layers. After following the software set-up guide given by CELLINK [35], the following settings were used in the CELLINK HeartWare slicer software for printing with the BIO X (table 2.5).

Table 2.5. CELLINK HeartWare slicer settings.

<i>Setting</i>	<i>Input</i>
Layer Height (mm)	0.410
First Layer Height (mm)	0.205
Extrusion Width (mm)	0.50
Vertical Shells (#)	1
Seam Position	Random
Infill (%)	70
Fill Pattern	Rectilinear
Skirt Loops (#)	0
Brim	None

The protocol for designing a cylinder matching these dimensions to result in a bioprinted construct were as follows:

1. Open Blender. In object mode, add a 'cylinder' mesh.
2. Increase the vertexes of the cylinder from 32 to 128.
3. Adjust the cylinder to the desired dimensions (20 mm x 20 mm x 1.5 mm).
4. Export to the .stl file format.
5. In CELLINK HeartWare, navigate to 'Slicer'. In the drop-down menu select 'PrusaSlicer'. Select 'Configuration' to open the slicer settings.
6. In the window that opens, add the .stl file.
7. Select 'Slice Now' and export the G-code to a USB flash drive for transfer to the BIO X 3D Bioprinter ready for bioprinting.

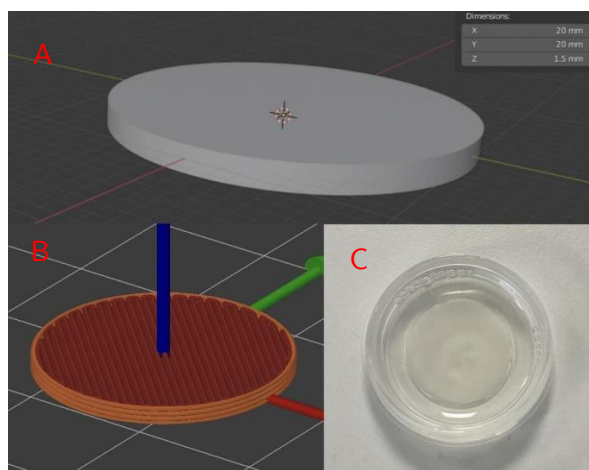


Figure 2.1. Bioprinted construct design process. A: Screenshot of design in CAD software Blender with dimensions shown. B: Screenshot taken in CELLINK HeartWare showing the effect of slicing and the 4 layers to be bioprinted. C: Image of bioprinted hydrogel construct in Ibidi 35 mm μ -dish.

2.2.4.2 Calibration Plates & Collagen Mold

A calibration plate was designed in Blender and printed on a Raise3D Pro2 Plus FDM printer to work in conjunction with the BIO X 3D bioprinter. This was required in order to perform bioprinting into the Ibidi 35 mm μ -dish. Additionally, in order to perform the collagen testing, a mold design was made. The following settings were used in the ideaMaker slicer software for printing with the Raise 3D Pro2 Plus 3D printer (table 2.6).

Table 2.6. ideaMaker slicer settings.

Setting	Input
Layer Height (mm)	0.10
Extrusion Width (mm)	0.44
Infill Density (%)	15
Support	None
Platform Additions	Raft Only
Raft Offset (mm)	5.00
Heated Bed Temperature ($^{\circ}$ C)	55
Extruder Temperature ($^{\circ}$ C)	210
Speed (mm/s)	50

Both were made from the following process:

1. Open Blender. In object mode, add a 'cube' mesh and adjust dimensions.
2. Transfer to edit mode and perform the necessary alterations to vertex points, edges and faces to create the final 3D object for printing.
3. Export to the .stl file format.

4. In ideaMaker, import the chosen .stl file. Select 'Start Slicing'.
5. In the main template settings select 'High Quality', then 'Slice' to obtain the G-code.
6. Export the G-code to a USB flash drive and transfer to the 3D printer to perform the final print.
7. Immediately after printing, place object into a sterile container until use.

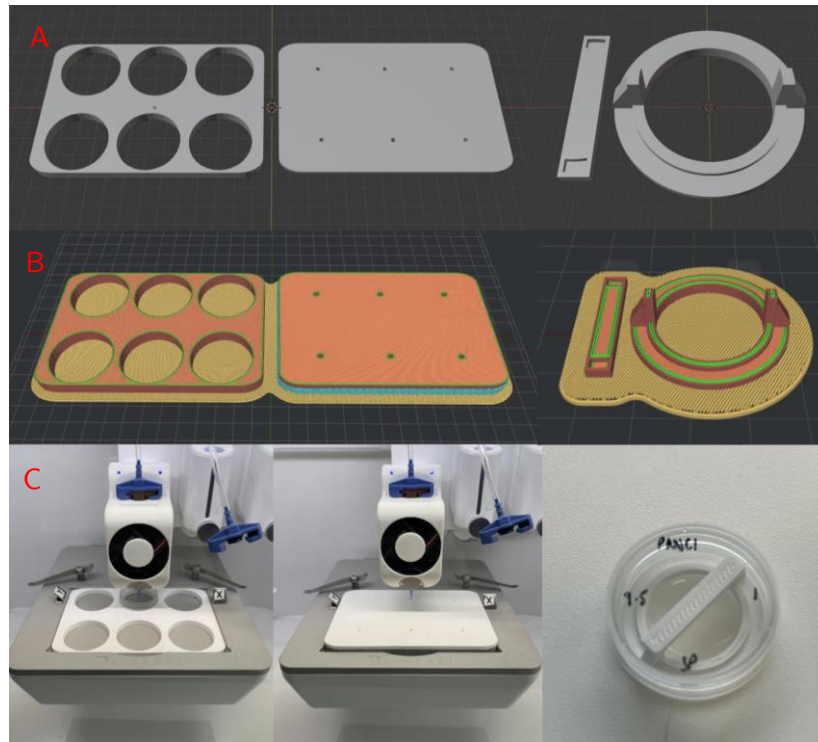


Figure 2.2. Calibration plate and collagen mold design process. A: Final blender designs. B: Sliced models in ideaMaker. C: Images taken of the final prints in use. Left to right: BIO X z-height calibration insert with μ -dish, manual start calibration plate, collagen mold.

2.2.4.3 Static Mixer Helix & 1 mL End Cap

To perform an efficient cell encapsulation a static cell mixer was designed from a modified 1 mL syringe and two resin printed objects, a static mixer helix and 1 mL end cap. The following settings were used in the PreForm slicer software for printing with the Formlabs Form 3B+ (table 2.7).

Table 2.7. Form 3B+ Settings:

Setting	Input
Material	Biomed White
Layer Thickness (mm)	0.050
Raft Type	Mini Rafts
Density	0.50
Touchpoint Size (mm)	0.20

The following design process was used to produce resin printed parts.

1. A pre-existing .stl file found online was imported into Blender.
2. In object mode, adjust the helix mesh to the desired dimensions (4.4 mm x 4.4 mm x 30 mm) for placement within a 1 mL syringe.
3. Export to the .stl file format.
4. In PreForm, import the chosen .stl file.
5. Adjust the orientation of the print on the printing surface.
6. Auto-generate support structures for the object, and edit as required.
7. Connect to the printer via ethernet and select 'Start a print'.
8. After printing, use the wash and cure stations to post-process the printed components. Using the wash station, submerge parts in 2-Propanol ($\geq 99.0\%$) for 20 min, then allow to air dry for 20 min.
9. After drying, place parts in a pre-warmed cure station (60 °C) and leave for 60 min to ensure a full cure.
10. Place finished printed parts in a sterile container.
11. Using a sharp edge, remove the end from a 1 mL syringe and combine resin printed parts to make a static helix mixer (figure 2.3).

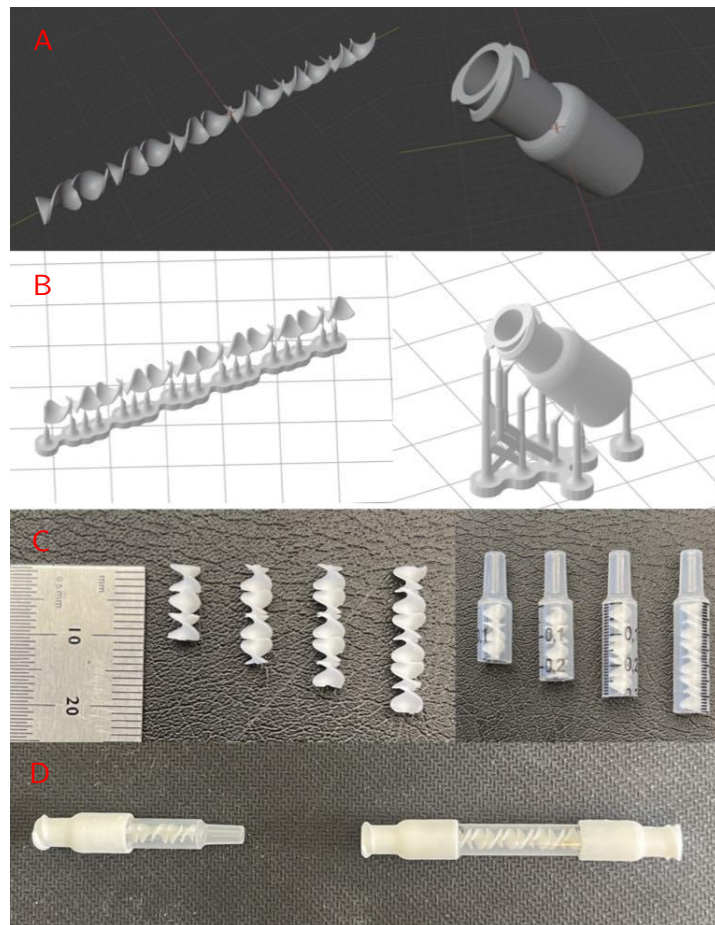


Figure 2.3. Static mixer design process. A: Final design in Blender. B: Sliced models in PreForm. C: Left; static mixer helix post-wash and cure. Right; static mixer helix inserted into modified 1 mL syringe. D: Post-autoclaved 1 mL static mixer designs with two design variants shown. The design on the left was used for all cell encapsulations in this thesis.

2.2.5 Bioprinting

The protocol to produce 3 hydrogel constructs for encapsulating cells within gels for subsequent printing, visualisation and rheology analysis is shown below.

1. Ready the BIO X by inputting the following.
 - a. 3D model: navigate to the .stl file (Rheology Disc.stl).
 - b. Print Surface: 'glass slide' was chosen for all experiments performed.
 - c. Printer Setup: Select temperature-controlled printhead, apply the UV curing settings and input required BIO X settings (table 2.8).
 - d. Layers: no changes were made.
 - e. Overview: confirm selected settings.
 - f. 3-Step Calibration:
 - i. Perform the auto-bed levelling
 - ii. Insert the calibration plate (figure 2.2C – left) containing an empty Ibidi 35 mm μ -dish and calibrate the z-height by manually, placing the printhead close to the glass surface of the dish.
 - iii. Using the second calibration plate (figure 2.2C – middle), manually select the starting position as directly in the middle of the centre μ -dish.
 - g. The BIO X is now ready to print. Proceed to cell encapsulation.
2. As per methods 2.2.1 – 2.2.3, resuspend PANC-1 cells in 200 μ L cDMEM. (For 2D cells, 11 million cells per 100 μ L were used. In hanging drop and microwell plate grown experiments, \approx 40 spheroids per 2 mL hydrogel were used.)
3. Remove Laminink from 4 °C storage and transfer from its CELLINK cartridge to a 3 mL syringe via a luer-lock adapter.
4. Heat the Laminink in a water bath set to 37 °C for 10 min. (For collagen, remove from 4 °C and use without heating).
5. Following CELLINK recommendations, ten parts hydrogel are to be mixed with one part cell suspension. To achieve this, in the experiments performed 2 mL of Laminink (or collagen) and 200 μ L cell solution were used.
6. Figure 2.4. shows the apparatus used for mixing. In order from left to right, connect the following: hydrogel in 3 mL syringe, static mixer, luer-lock adapter, 200 μ L cell solution in 1 mL syringe.
7. Pre-fill the static mixer with the hydrogel, then gently apply alternating pressure between syringes to mix and encapsulate the cells within the hydrogel.
8. Transfer the cell-laden hydrogel from the 3 mL syringe to the CELLINK cartridge using a luer-lock adapter. (For collagen, the cell-laden hydrogel was added to a μ -dish containing a printed collagen mold (figure 2.2C – right), and then placed into an incubator for 1 hour. Once the gel had set, the 3D printed

- plastic mold was removed, 1.5 mL imaging media added, and the hydrogel construct replaced in the incubator).
9. Place the 3 mL BIO X cartridge containing the hydrogel into the BIO X and start the print.
 10. During printing, the flow of material was monitored and the kPa pressure exerted onto the cell-laden hydrogel in the BIO X cartridge was adjusted to try to maintain as constant as flow as possible.
 11. After printing, 1.5 mL CaCl_2 was added for 30 s of ionic crosslinking. After the 30 s, the CaCl_2 was removed and the construct washed with X1 PBS. After washing, the hydrogel constructs were submerged in 2 mL imaging media and placed into an incubator (37°C , 5% CO_2).

Table 2.8. BIO X settings.

<i>Setting</i>	<i>Input</i>
Nozzle Size (Gauge)	22G
Extrusion Pressure (kPa)	7 - 15
Pre-Flow (ms)	20
Post-Flow (ms)	10
Syringe Temperature ($^\circ\text{C}$)	24
Printbed Temperature ($^\circ\text{C}$)	15
Printing Speed (mm/s)	4
UV Module (nm)	405
UV Crosslinking Events (#)	1
UV Time (s)	15.4
UV Intensity (%)	100
Ionic Curing Volume (mL)	1.5
Ionic Curing Time (s)	60
Cell to Ink Ratio	1:10

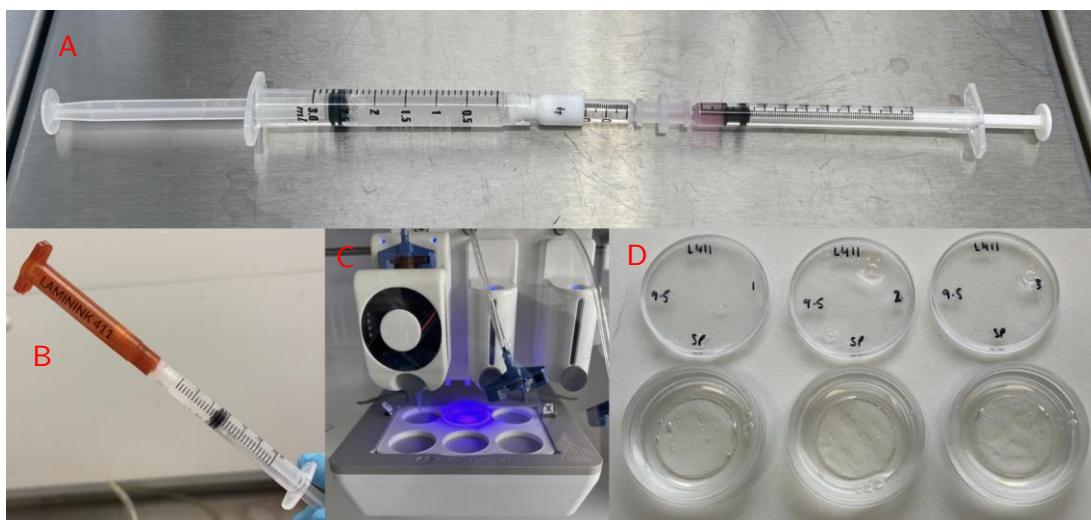


Figure 2.4. A: Cell encapsulation apparatus. B: Transferring cell-laden hydrogel to 3 mL CELLINK cartridge. C: Post-print curing on the BIO X. D: Final bioprinted constructs.

2.2.6 Live Cell Imaging

Bioprinted hydrogel constructs were removed from the incubator and placed into a sterile fume cabinet. Using a pipette, the cell media was removed and replaced a 1.5 mL pre-prepared solution of calcein and mitotracker deep red in imaging media, both of which were diluted to 1:2000. The hydrogels were placed into the incubator for 40 min, after which the imaging solution was removed. During this incubation, the Leica SP8 confocal microscope was turned on and a calibration Ibidi 35 mm μ -dish was used to set up the instrument ready for imminent visualisation. After incubation, the constructs were washed twice with X1 PBS and 1.5 mL imaging media was added to prevent the gels from drying out. In order to limit cellular stress, imaging was performed on constructs containing cells individually. After a hydrogel was imaged, it was placed back into the foil-lined container and transferred back to the incubator. Only a single hydrogel construct was active outside of the incubator at a time.

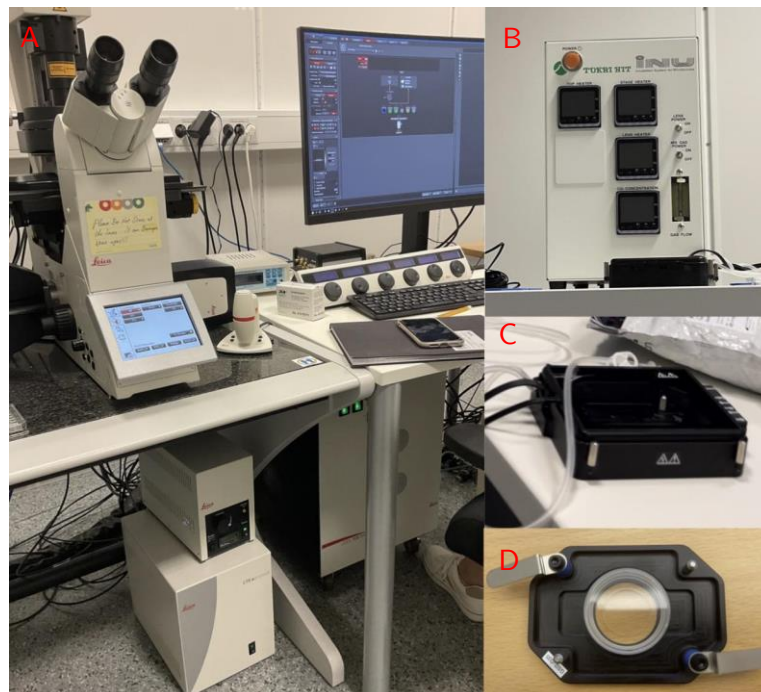


Figure 2.5. Live cell imaging equipment used. A: Leica SP8 confocal microscope with computer, control box, electronic and laser power. B, C: Tokai hit incubation system. D: Microscope insert to μ -dish.

2.2.7 Characterisation of Mechanical Properties

A DHR-2 rheometer by TA instruments was used. In order to limit cellular stress, mechanical testing was performed on constructs containing cells individually. A single construct was removed from the incubator and transferred to the rheometer for testing via a foil-insulated container. As soon as the probe had finished

performing the mechanical test, the hydrogel construct was placed back into the Ibidi dish with care and transferred back to the incubator. At this point the second sample would be taken and transferred to the incubator. In order to provide reproducibility to the results, it was aimed that a minimum of 3 samples would be tested in this way. For all rheology measurements, the settings applied in TRIOS for use with the DHR 2 are shown in Table 2.9.

Table 2.9. Settings applied for rheological analysis of hydrogel constructs.

Setting	Oscillation Amplitude	Frequency Sweep
Frequency (Hz)	1.0	5.0 to 0.01
Strain (%)	0.01 to 200	1.0
Axial Force (N)	≤ 0.3	
Temperature (°C)	25	
Loading Gap (μm)	50,000	
Geometry	20 mm Parallel Plate XHATCH	
Gap (μm)	Variable (between 1500 and 37) *	

*Refer to technical challenges.

Following the created procedure file, the samples were loaded onto the surface of the rheometer and the experiment was run. In order to account for the gap size difference between Laminink and collagen hydrogels, the probe was manually lowered until the probe registered an axial force of ≈ 0.3 N, at which point the measured gap size was inputted into the experimental set up. After running a sample, the rheometer probe was raised automatically, allowing retrieval of the hydrogel construct. The probe gap was zeroed after every sample run. Once finished, samples were carefully removed and placed back into their original containers for disposal following approved methods. Appropriate PPE was worn. Probes and surfaces were sterilised with 70 % ethanol after use.

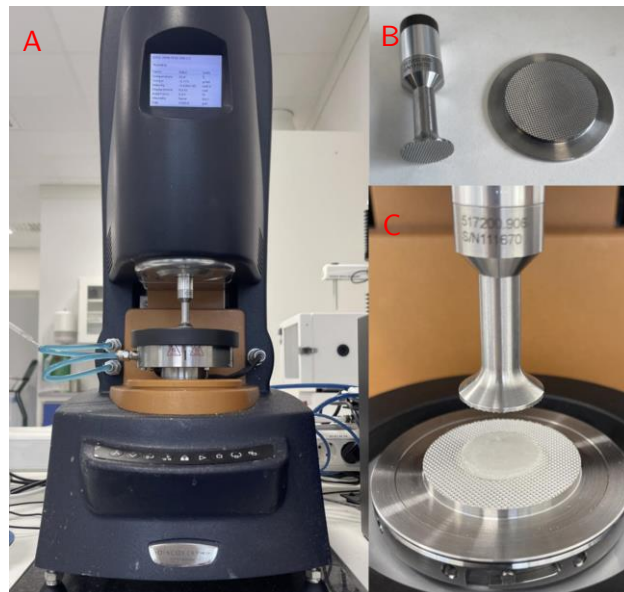


Figure 2.6. Mechanical testing equipment used. A: TA Instruments DHR-2. B: Crosshatched 20 mm peltier plate and lower platform. C: Laminink hydrogel positioned on DHR-2 prior to analysis.

2.2.8 Data Analysis

Imaging data was handled using LAS X software. Images were visualised and slight adjustments to the brightness of the fluorescence were made to improve their visual quality within LAS X. Scale bars were added within LAS X for the spheroid fragments observed and the PANC-1 cluster (figure 3.3 and 3.4).

For the rheology measurements, the DHR-2 software TRIOS was used. Within TRIOS, oscillation amplitude data from tests performed were collated into 'overlay' documents. Within these documents the raw data could be obtained. Raw data was exported to excel and the average storage modulus was calculated to produce the oscillation amplitude graphs (figure 3.1 and 3.5). From the linear region in these graphs the strain % for use in the frequency sweep tests was determined.

For the frequency sweep measurements taken on hydrogel constructs, the results were collated in TRIOS into an overlay document. Within the overlay document for the frequency sweeps, TRIOS's straight-line analysis function was used to obtain the straight-line slopes for each result. As stated in a previous study, "the slope of the linear region represented the value for Young's Modulus", this is another title for matrix stiffness ^[36]. These results were in MPa so to convert to kPa the slope values were multiplied by 1000, producing the final kPa values for matrix stiffness. Matrix stiffness results (in kPa) were averaged to give the final results.

Chapter 3

Results

Laminink hydrogel construct results are presented as a progression of experiments of increasing complexity. Results from the collagen hydrogels are presented collectively.

3.1 Laminink Hydrogels

3.1.1 Bioprinted Construct for Cell Viability and Viscoelasticity Testing

Three Laminink rheology discs were produced and the average oscillation amplitude results were used to taken using the DHR-2 (Figure 3.1).

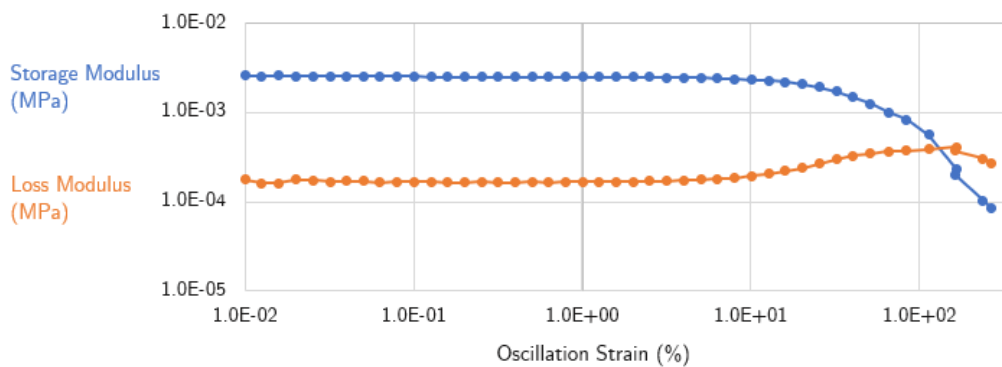


Figure 3.1. Oscillation amplitude results of Laminink rheology disc showing the viscoelastic region between 0.01 and 300 % oscillation strain.

The viscoelastic region, identified in figure 3.1 as the straight-line region between 0.01 and 300 % oscillation strain, showed that for the Laminink material a strain of 1.0 % would be acceptable for all future frequency sweep measurements.

3.1.2 CELLINK Recommended Settings

A protocol provided by CELLINK which stated the recommended settings for their GelXA Laminink 411 hydrogel was followed in order to determine whether future experiments would use either the 365 nm or 405 nm wavelength of light for crosslinking (table 3.1)^[34]. UV crosslinking was applied once, after the 4th printed layer and above the centre of the hydrogel. From the oscillation sweep, 1.0 % strain was used in the frequency sweep measurements. Results for Laminink hydrogels crosslinked at 365 and 405 nm gave kPa values 40.9 and 0.11 kPa respectively (figure 3.2). Straight line slopes results were averaged and multiplied by 1000 to translate results from complex modulus MPa into kPa. Mechanical testing was performed approximately 1 day after bioprinting.

Table 3.1. CELLINK Laminink 411 recommended settings.

Wavelength (nm)	Time (s)	Height (mm)	Light Intensity (%)
365	8.8	50	100
405	15.0	50	100

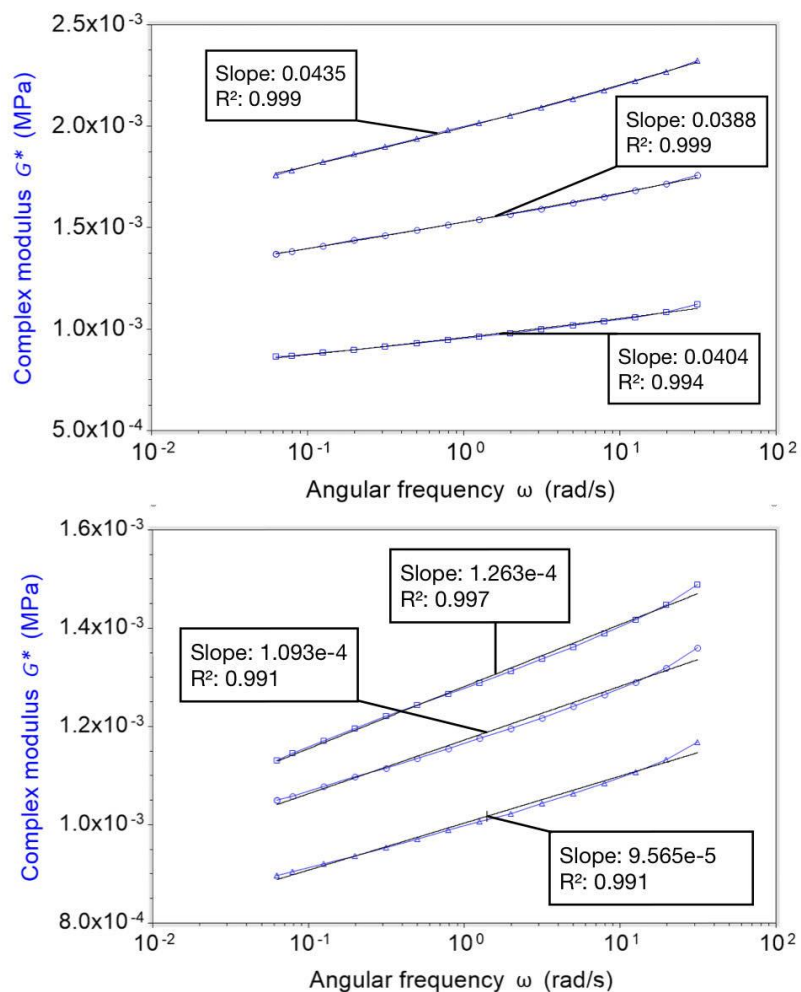


Figure 3.2. Laminink frequency sweep results with 405 nm crosslinking.

3.1.3 A 405nm Crosslinking Guide

In order to mimic pancreatic tumor tissue, the ideal kPa region of the Laminink would have to be close to 4 ± 2 kPa [27, 30, 31]. To aim for this, it was necessary to design a method by which the UV crosslinking could be adjusted. The following crosslinking optimisation guide for the 405 nm UV module was designed. Using the surface area of a 20 mm disc (314 mm^2), measurements of the UV modules cone of light from pictures taken at specific heights and the principles of beam theory, a theoretical value of the radiant flux (RF), in $\text{mW}/\text{mm}^2\cdot\text{s}$, at all BIO X module heights was calculated (Appendix). In experiment 2, for example, theoretically 405 nm at 50 mm for 15 s would equal an RF value of $58.65 \text{ mW}/\text{mm}^2$.

Table 3.2. BIO X 405 nm crosslinking guide.

<i>Height (mm)</i>	<i>Average Intensity on a Surface Area of 314mm^2</i>	<i>Average Radiant Flux on a Surface Area of 314mm^2</i>	<i>Radiant Flux ($\text{mW}/\text{mm}^2\cdot\text{s}$)</i>
40	93.9	1900.6	5.90
41	94.3	1816.8	5.64
42	94.6	1738.5	5.40
43	95.0	1665.1	5.17
44	95.4	1596.3	4.96
45	95.7	1531.7	4.76
46	96.1	1471.0	4.57
47	96.4	1413.7	4.39
48	96.7	1359.7	4.22
49	97.0	1308.7	4.06
50	97.3	1260.5	3.91
51	97.5	1214.8	3.77
52	97.8	1171.5	3.64
53	98.0	1130.4	3.51
54	98.2	1091.3	3.39
55	98.4	1054.2	3.27
56	98.6	1018.8	3.16
57	98.8	985.1	3.06
58	98.9	953.0	2.96
59	99.1	922.4	2.86
60	99.2	893.1	2.77
61	99.4	865.1	2.69
62	99.5	838.3	2.60
63	99.6	812.7	2.52
64	99.6	788.1	2.45
65	99.7	764.6	2.37

3.1.4 Getting Closer to 4 kPa

By considering the RF value from the CELLINK recommended settings as a baseline of 100 % the heights and times of the UV module required to achieve an increase in RF equivalent to 200 and 400 % with respect to the baseline of experiment 2 were determined (table 3.3) in order to try to improve the kPa from 0.11 closer to 4 kPa.

Table 3.3. Laminink UV crosslinking optimisation calculated from RF.

<i>Height</i>	<i>RF (mW/mm²·s)</i>	<i>UV Crosslinking Time (s)</i>	<i>Times Crosslinked</i>	<i>Total RF (mW/mm²·s)</i>	<i>RF increase with respect to original (%)</i>
50	3.91	15.0	1	58.61	100.0
40	5.88	19.9	1	117.10	199.8
40	5.88	19.9	2	234.20	399.6

Mechanical testing was performed on days 1, 7 and 14 to gauge the resilience of the Laminink hydrogels and as a proof of principle for the bioprinting workflow. By increasing the RF (%) to the settings of the BIO X when printing the designed discs, the kPa increased to over 40 across all timepoints measured.

Table 3.4. Matrix stiffness in kPa for Laminink hydrogels at 200 % and 400 % RF increase.

<i>RF (%)</i>	<i>Matrix Stiffness (kPa)</i>		
	<i>Day 1</i>	<i>Day 7</i>	<i>Day 14</i>
200	40.16	42.06	41.60
400	40.78	43.72	49.46

3.1.5 2D PANC-1 Encapsulation

With both 200 % and 400 % increases clearly showing higher than intended crosslinking, the RF relative increase was lowered to 125 % by increasing the module height to 45 mm and decreasing the time to 15.4 s (table 3.5). Due to the lack of available Laminink material, cells had to be included at this point of the project. This unfortunately meant that no negative controls could be made from this point onwards. The following UV crosslinking settings were used for the remainder of the project.

Table 3.5. UV settings used for all cell-laden Laminink hydrogel constructs.

<i>Height</i>	<i>RF (mW/mm²·s)</i>	<i>UV Crosslinking Time (s)</i>	<i>Times Crosslinked</i>	<i>Total RF (mW/mm²·s)</i>	<i>RF increase with respect to original (%)</i>
45	4.76	15.4	1	73.30	125

Using PANC-1 cells cultured in standard 2D cell culture flasks, cells were mixed with Laminink and after incubation for 1-day confocal imaging and rheology was performed. The workflow was repeated after day 7. Both images show high cell viability in these hydrogels. The formation of PANC-1 clusters is visible (figure 3.3).

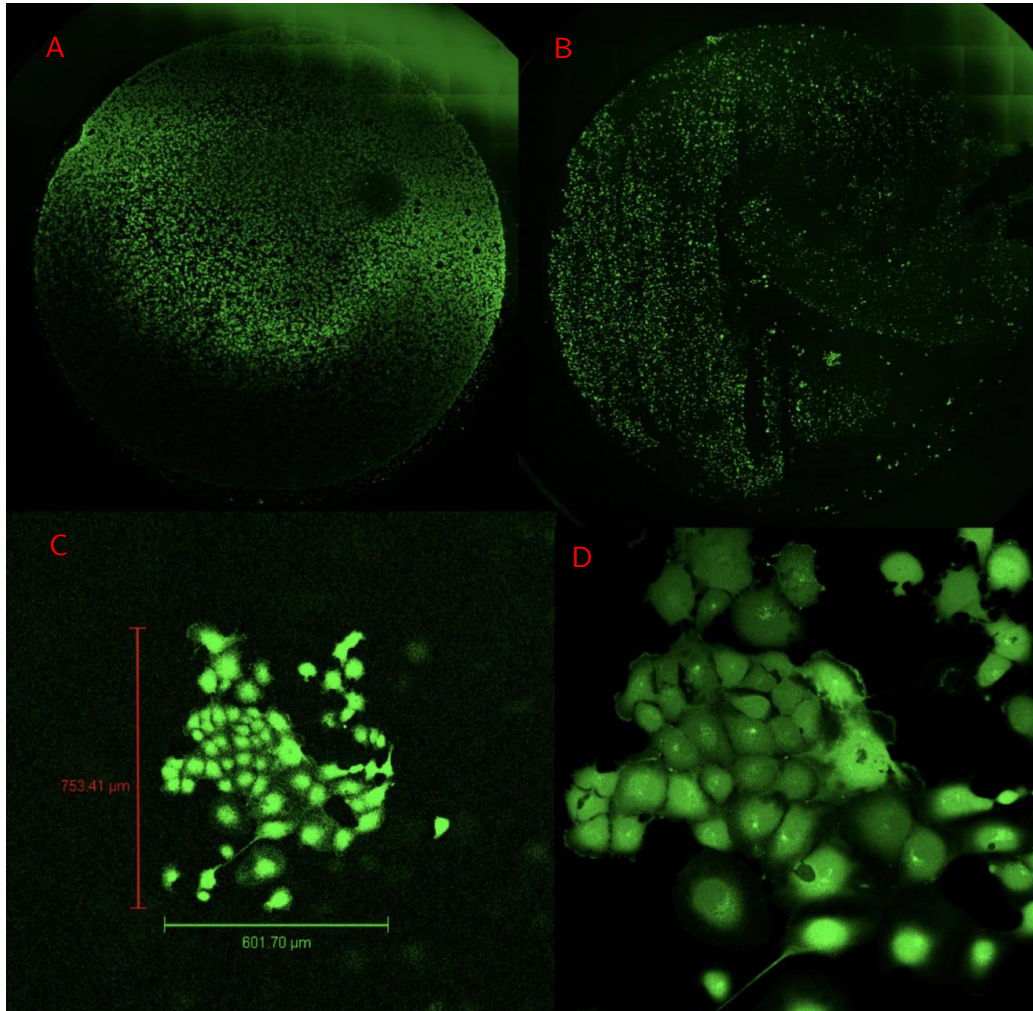


Figure 3.3. Image of viable PANC-1 cells on day 1 (A) and day 7 (B) in a Laminink hydrogel construct bioprinted using the BIO X obtained on a Leica SP8 confocal microscope. C: Multicellular PANC-1 cluster taken with X20 objective lens (approximate size: 750 × 600 μm). D: PANC-1 cluster image taken with X63 objective lens.

Results from the rheology showed high matrix stiffness ranging between 34 – 51 on day 1 and 45 – 59 on day 7 (Table 3.6). To assess the matrix stiffness across the two different time points and with cells imbedded an oscillation sweep was performed.

Table 3.6. Matrix stiffness of Laminink hydrogels encapsulated in 2D PANC-1 cells.

Hydrogel	Matrix Stiffness (kPa)	
	Day 1	Day 7
1	34.64	45.48
2	56.70	57.49
3	51.42	58.68

3.1.6 Hanging Drop Spheroids Encapsulation

An investigation into the usability of hanging drop spheroids was performed. Unfortunately, the image that was returned from the confocal microscope was completely black, and therefore from the absence of fluorescence cell viability could be regarded as zero. Mechanical testing on the single construct made gave a matrix stiffness value of 61.75 kPa for the hanging drop hydrogel construct.

3.1.7 Microwell Spheroids Encapsulation

Using a 96-microwell plate designed for the culture of spheroids. PANC-1 cells were grown for 10 days and encapsulated with Laminink. As per the workflow, imaging was performed on day 1 to produce the following images (figure 3.4).

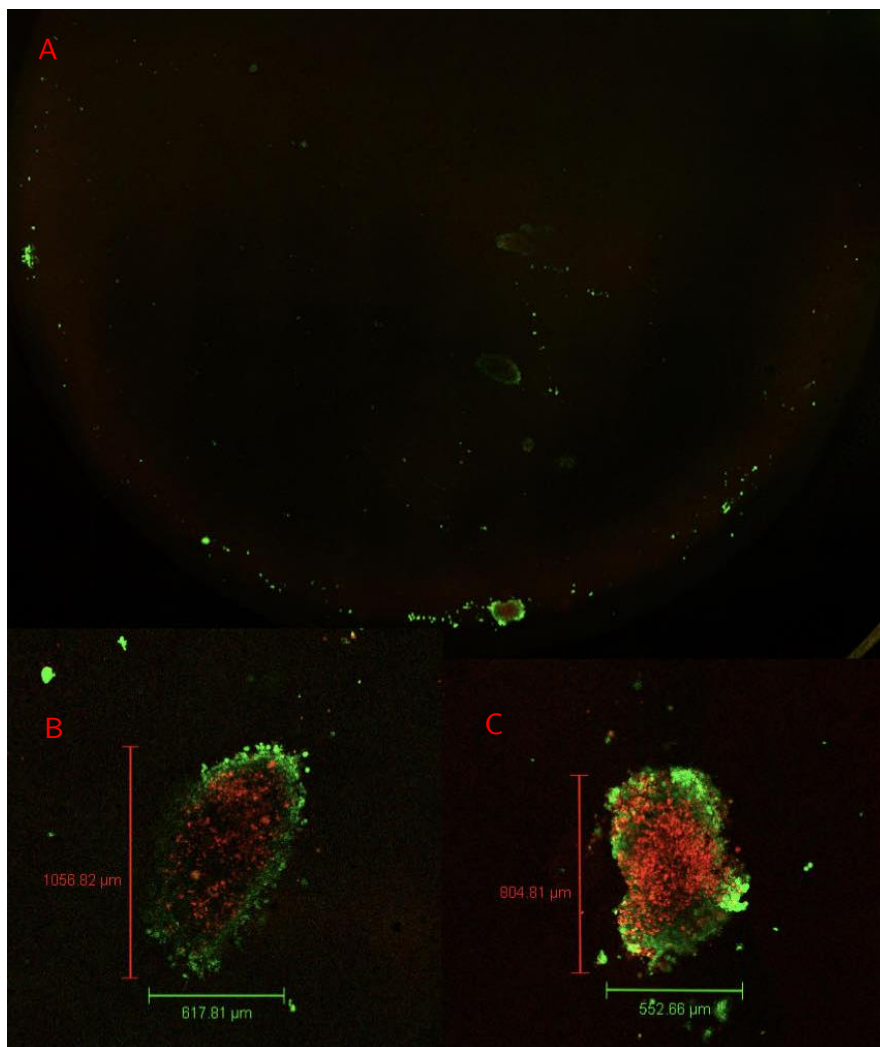


Figure 3.4. A: Surface area scan of an Ibidi 35 mm μ -Dish containing microwell plate grown PANC-1 spheroids in Laminink 411 using a X5 objective on a Leica SP8 confocal microscope showing the viability of PANC-1 spheroids after bioprinting on the BIO X. B, C: PANC-1 spheroids encapsulated in Laminink 411 hydrogel and bioprinted using the BIO X. Objective lens X20. Approximate sizes: B – 1050 \times 620 μ m; C – 800 \times 550 μ m.

Two hydrogel constructs were made and rheological testing was performed after 1 day. An average matrix stiffness of 49.21 kPa was measured between the two hydrogels (table 3.7).

Table 3.7 Matrix stiffness of Laminink hydrogels encapsulated with microwell plate grown PANC-1 spheroids.

Hydrogel	Matrix Stiffness (kPa)
1	45.36
2	53.06

3.2 Collagen Hydrogels

Oscillation amplitude on 3 collagen hydrogel constructs showed a near viscoelastic region at 1% strain (figure 3.5). In the frequency sweep testing, 1% strain was used to determine the matrix stiffness, in kPa. The average of the slopes in the frequency sweep equalled 0.145 (figure 3.5). Translation of this result to an averaged matrix stiffness gave 145 kPa for the collagen hydrogel constructs tested (table 3.8).

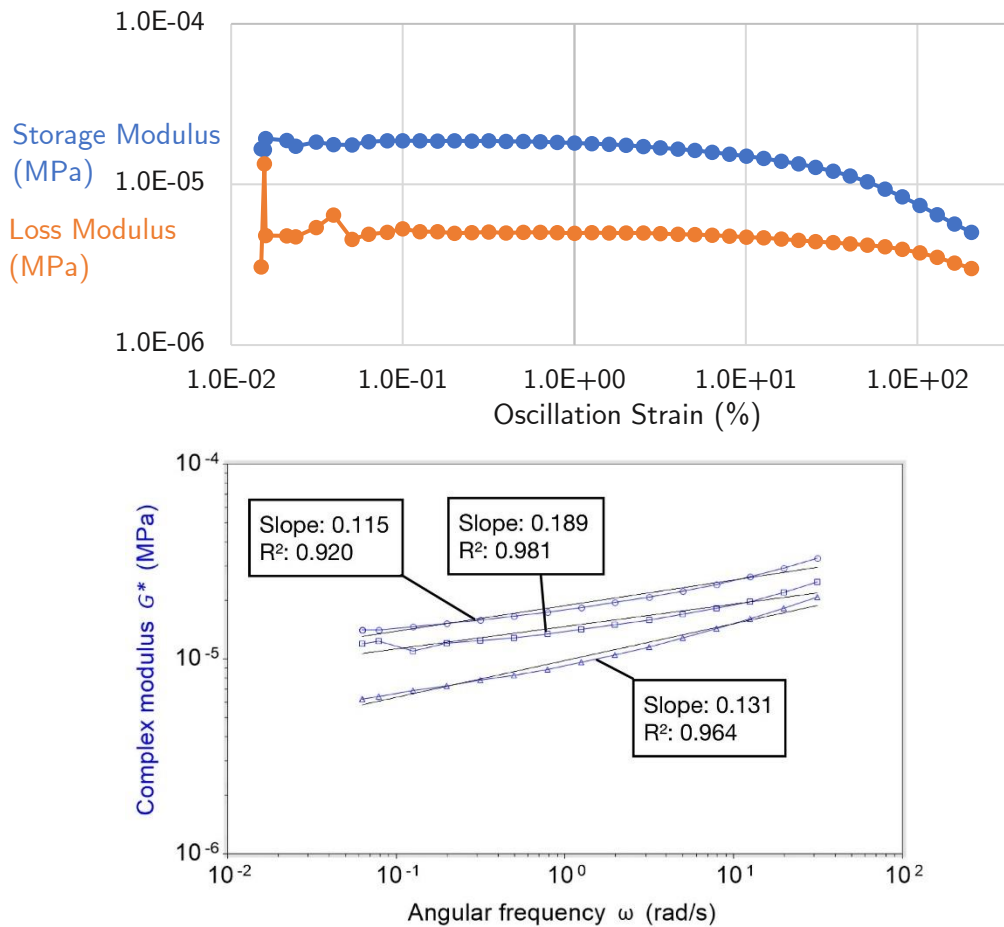


Figure 3.5. Averaged oscillation amplitude and frequency sweep test results of 3 collagen hydrogels. Above: oscillation amplitude results. Below: Frequency sweep results.

Table 3.8. Collagen hydrogel construct mechanical testing results.

Hydrogel	Matrix Stiffness (kPa)
1	115
2	189
3	131

Live cell imaging on the collagen hydrogels was performed 1 day after formation (figure 3.6).

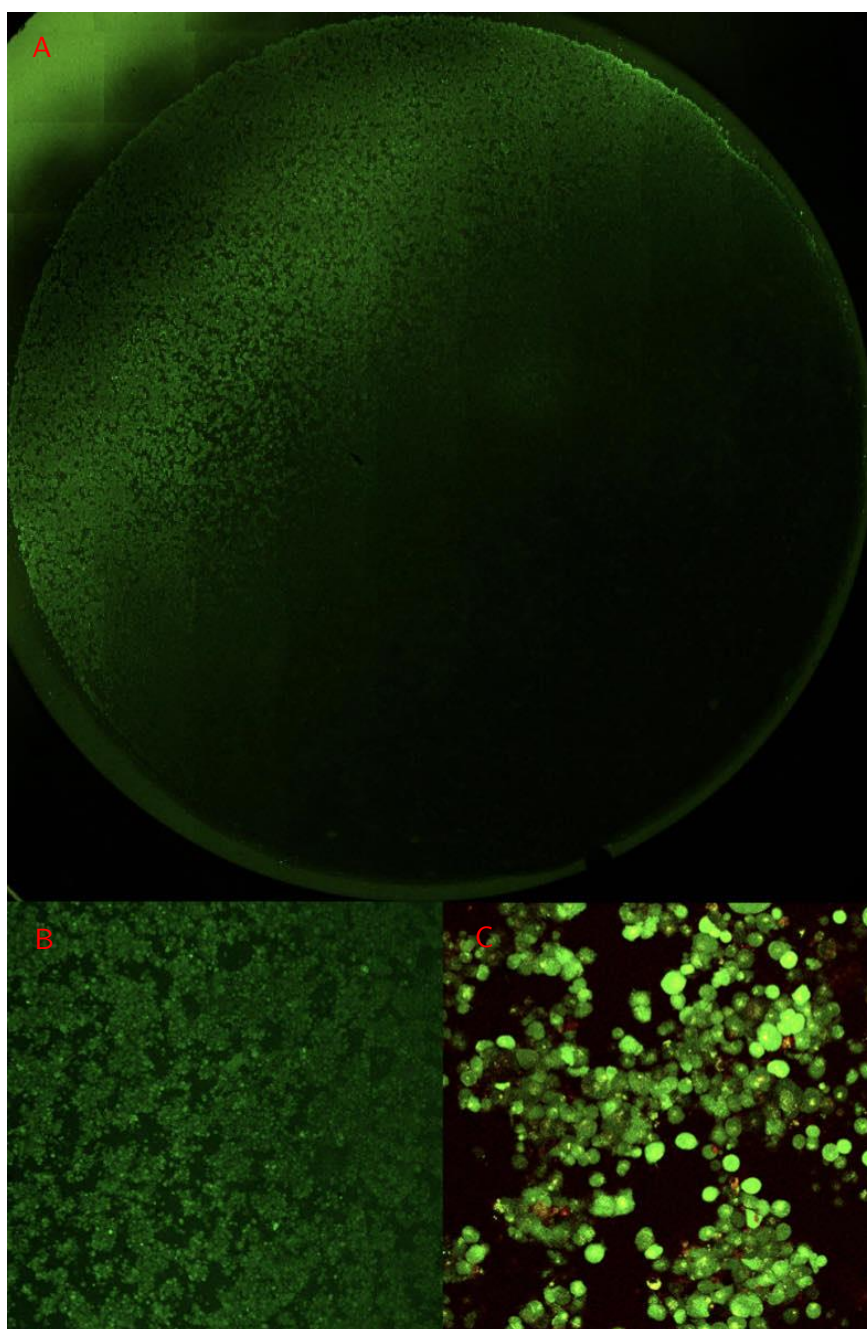


Figure 3.6. Live cell images of collagen hydrogel construct in Ibidi μ -dish 1 day after production taken with Leica SP8. A: Surface area scan of the μ -dish taken with X5 objective. B: Section of collagen hydrogel taken using X20 objective. C: PANC-1 cells of high viability in collagen hydrogel, taken with X63 objective.

Chapter 4

Discussion

4.1 Summary and Interpretation of Results

At the onset of the investigation into the potential useability of Laminink, the 365 nm module was discarded as the crosslinking resulting from this stronger UV wavelength resulted in a kPa value far outside the ideal range. The 0.11 kPa result obtained from the CELLINK recommended settings at 405 nm was promising as this suggested improvement towards 4 kPa could be achieved with relative ease. The 405 nm module was then selected for all future experiments. It was thought that increase the UV crosslinking strength, from an increase in RF calculated would result in a modest increase – however this was not the case. The results obtained in 3.1.4 both resulted in stiffnesses well over what was intended. That the 200 % and 400 % RF increased hydrogel constructs both showed kPa around 40 and combined with the kPa results obtained from results 3.1.5 (with 125 % RF) are again around 40 kPa, the following observation on Laminink may be suggested. The window to achieve controllable Laminink crosslinking aiming for a range between 0.11 kPa and values of kPa lower than 40 is a small one. That the ionic crosslinking in CaCl_2 was performed on all hydrogels throughout would rather have not been performed in the experiments – as this may have resulted in a lower degree of crosslinking - but due to the authors chosen experimentation method, the primary parameter to be changed to elicit control over Laminink was the UV crosslinking. Therefore, UV time and height were adjusted seeking control over the mechanical properties over the material and not ionic control. Ionic crosslinking may provide more control over the ability to obtain a kPa for Laminink in the range required to mimic pancreatic cancer tissue compared to UV crosslinking control. Ionic crosslinking only, with no use of the UV modules was not tested.

Nevertheless, the experiments proceeded with a downgraded UV crosslinking at 125 % RF value with UV module operation time at 15.4 s and height 45 mm. The results of all imaging experiments in Laminink, from the images obtained, clearly show the viability of PANC-1 cells in this material, even with the high matrix stiffnesses. Standard 2D culture after 7 days showed the presence of a clearly

visible cluster of PANC-1 cells. That this cluster developed shows the suitability of Laminink as a matrix mimic, such that the cells can orientate themselves to migrate into clusters such as these. Cell adhesion between cells and further development of the cluster could allow for further investigations to be performed.

In the hanging drop PANC-1 spheroid encapsulation, as stated in 3.1.6, no fluorescence was detected when visualising by the same means as all other constructs imaged. The bioprinting process on these cells was not successful. A number of reasons may account for this, perhaps the spheroids themselves were not in a high state of viability before encapsulation. During the encapsulation and mixing procedure in the fume hood in this experiment, there was an experimental error when the Laminink was mixed with the PANC-1 cells. In this experiment, the Laminink was not transferred to a 3 ml (2.2.5, step 3) and the CELLINK cartridge instead was used to encapsulate these cells. It should be noted that this was the first time the encapsulation was performed. During this, the CELLINK cartridge was connected to the 200 μ L hanging drop spheroid containing solution in a 1 mL syringe and the pneumatic mixing was performed. Without the presence of a pump on the CELLINK cartridge, it proved difficult to mix the cells together resulting in a messy, incomplete encapsulation process. Material loss as a result of this and incomplete mixing resulted in the formation of a single hydrogel construct when the production of three was intended with the material present. The presence of cells within the lost material may have been the cause of the lack of visible cells observed. That the extremely high kPa of 61.75 measured from the hydrogel produced may have also been involved in the lack of viability, a value such as this is greatly over what was intended during Laminink experiments.

In the microwell spheroid encapsulation, the two aggregates of PANC-1 cells that formed from the spheroids used in the experiment show that large cellular structures are able to survive the bioprinting process (figure 3.4). An interesting observation from the imaging of these hydrogel constructs are what appears to be a caveat of bioprinting. That heavy cellular structures in biomaterial can settle, under gravity, to the bottom of the hydrogel container – in this case the 3 mL CELLINK cartridge. During the bioprinting of the hydrogel constructs, with the way that the G-code was created from CELLINK HeartWare the outer perimeter of the hydrogel construct prints first. In the visualisation of the construct (figure 3.4) the majority of cells appear to be present at the outskirts. That the spheroids encapsulated in the Laminink had settled to the bottom of the cartridge, and that printing occurs at the outskirts of the construct first, would account for this. The presence of a PANC-1 aggregate near in the centre does show that not all cells are deposited at the outer perimeter, but clearly in the image most cells are. This potential issue would need to be considered when performing spheroid-encapsulations, especially if the hydrogel material, like the collagen used in these experiments resembles a liquid before gelation. The complete failure to achieve a

kPa in any of the hydrogels anywhere near to 4 kPa is a disappointing result. Inexperience with instruments, non-optimisation of the bioprinting and crosslinking processes, printability of the Laminink and the lack of material for testing are all important causative factors. Control to achieve 4 kPa was only really tested with the use of the UV module, and other methods or the absence of UV crosslinking itself may have proved more useful. Further experience with the DHR-2 and settings in the procedure used may be required to achieve more accurate results.

Initial collagen experiments were unable to induce gelation in the μ -dish. The use of a printed mold to be placed in the μ -dish was tried and proved successful. Removal of the printed object from the μ -dish left a collagen hydrogel disc similar to the bioprinted Laminink albeit with a significantly reduced z-height. These gels were tested the same as the Laminink and the imaging experiments were successful. Viability was shown in these cells and their composition was extremely homogenous (figure 3.6). That the collagen was essentially a liquid during the mixing aided in this process, and air bubbles could be eliminated using hand-induced centrifugal force on the syringe with relative ease. A process for the Laminink which proved much harder to achieve. With the gels produced, rheological testing results are clearly too high and cannot be considered as accurate results. The kPa values obtained would present a material of such an extreme degree of stiffness, and the collagen hydrogel constructs were anything but. They were very flexible materials. The results must be as a result of the incomplete optimisation of the rheological testing. As the method for rheological testing was a modified version of the Laminink protocol, a unique method for testing the collagen hydrogel constructs may have needed to be developed.

4.2 Bioprinting Optimisations

Any researcher wishing to delve into the process of bioprinting and hydrogel development needs to first familiarize themselves with method 2.2.5 and table 2.8. As can be seen from the bioprinting procedure and settings, the scale of optimising parameters in bioprinting is extremely large – this perhaps presents the greatest challenge. The main consideration about how to resolve the issues experienced in the thesis would be from considering the bioprinting method and the setting optimisation that can be achieved on such an instrument as the BIO X.

That the characteristics and the nature of each bioprinting material are unique, should make it clear to researchers that development in this field is by no means a process which can be done in a short time frame. In order to achieve a fully realised version of a material that can be used in the study of pancreatic cancer is a drawn-out process, and assessing knowing how to work with such materials also requires extensive testing.

The following parameters present some bioprinting development considerations with the BIO X (table 4.1).

Table 4.1. BIO X parameters, modifications and considerations when bioprinting.

<i>Parameter</i>	<i>Modifications</i>	<i>Considerations</i>
Nozzle size	Nozzles or Needles 18G, 20G, 22G, 25G, 27G	Changes made here improve any potential resolution, however the speed of printing and slicer settings would need to be adjusted as a result.
Extrusion pressure	1 - 700 kPa Increments of 1 kPa	Controllable via the light emitting diode (LED) touchscreen. Has to be constantly monitored during printing. In the work performed, Laminink was printed between 6 - 20 kPa. Single kPa changes can result in large difference in flow rate. Changes in 0.1 kPa would provide greater control.
Pre-flow and Post-flow	Increments of milliseconds	Essential in achieving proper flow, adjustments here are very material specific. Extensive work would need to be performed here alone per material. Optimisations here improve replication of the slicer G-code.
Temperature-Controlled Printhead	Low: 4 C High: 65 C	Important in improving printability.
Printbed temperature	Low: 4C High: 60 C	Aids in crosslinking of temperature-constructs. Time of construct on cooled surfaces.
Printing speed	Increments of 0.1 mm/s	Improvements here are significant if printing multiple constructs. As it can be 5 min for one construct, consider the down-the-line time effects such as potential gravity-mediated dropout of larger cellular structures. At least 3 constructs need to be printed for repeatability. However, 5 and more would be preferred.
Crosslinking events	Number of events per layer	Material specific UV penetration. Effects of UV on top layer compared to lower layers, and the combined effect of multiple crosslinking events.
LED (and UV) modules	365, 405 nm UV modules 485, 520 nm LED modules	BIO X provides a nice range of modules. Custom UV selection may be a worthwhile future consideration.
UV time	Increments of 0.1 s	All must be taken together to control UV crosslinking. Possible combinations of each to elicit control are high. Accurate values for mW/mm ² would provide better adjustment of these to elicit more control over UV crosslinking.
UV intensity	0 - 100 % possible	
UV height	40 - 60 mm	
Ionic curing volume and time	Post-processing adjustment	Volumes and times are highly adjustable post-printing.
Cell to ink ratio	1:10 and all other possibilities	Potential positive effects on kPa and ease of printability.
Bioprinting layers	Defined by model height and slicer settings	Determined by testing methods of final bioprinted construct. Important in determining UV events.

4.3 Technical Challenges

The establishment of this bioprinting workflow with the use of approximately 27 mL of Laminink material was one of the largest challenges in the work performed. Mixing methods and material losses during multiple encapsulation events resulted in the incomplete production of the three hydrogels required to ensure proper reproducibility. In some experiments, three hydrogels could be prepared but for some others only the production of a single bioprinted construct could be made. The issue is that of capacity. Bioprinting is a process which, as already described, requires immense optimisation, and as such there needs to be an available source of material to work with. The fact that in this study the Laminink cartridges contained 3 mL of material, and that the number of cartridges was again limited was not an ideal basis for any form of bioprinting development or assessment.

Maintaining a gap height during the rheology analysis is a highly challenging process and as such the gap height during rheology had to be varied (Table 2.9). Non-homogenous flow of material and slightly different calibration heights on the BIO X meant that the production of rheology discs with an exact height of, for example, 1000 μm was one of the largest challenges presented. During bioprinting, constant alterations to the air pressure extruding the bioink had to be made manually in order for the material flow to be kept constant throughout the production of the three bioinks required for a complete reproducible experiment to be performed. Whilst the BIO X is capable of delivering pressure changes in intervals of 1 kPa, the ability to perform changes of 0.1 pKa, if possible, is something that would be advantageous in order to exert greater control over the prototyping phase of bioink production or in the analysis of a small volumes of highly costly material such as GelXA Laminink 411.

Issues surrounding the process of imaging, mainly getting the prints to lay flat for imaging were an additional challenge. The fact that bioprinters can be used to deposit material on the surface of the glass μ -dish microscope slide meant that imaging with the Laminink was generally easy to achieve, as the bioprinted material for study was placed directly on the surface of the microscope slide. The addition of material, and the exposure of the entire surface area of the bioprinted discs to the imaging solution containing the trackers meant that often the hydrogel constructs would rise from the surface and float in the middle of the μ -dish. This meant that the media had to be removed prior to use, necessitating further workup that would ideally have been avoided. With the media removed the prints were laid flat on the surface again, but not ideally. Figure 3.3A and 3.6A show a non-flat orientation of the printed construct, with cell viability on the surface scan only showing a section of the print and not the entire surface area as intended.

Due to the nature of the BIO X, that it is G-code based and works exactly in the same manner as FDM 3D printers there exists the technical challenge of controlling

the instrument. Colloquially it is informally known as 'gremlins' or 'ghosts', almost all versions of 3D printing technology contains small software issues that can result in a print failure. An example of this occurred during the work performed. After the lengthy process, involving many steps, to achieve a bioprinted construct was performed with the limited material available it transpired that during UV crosslinking on the BIO X the UV module decided to position itself away from the centre of the construct. That this occurred meant that the construct was crosslinked improperly and as such no useable data could be obtained as with the BIO X, in essence, there is one opportunity to get the crosslinking right based on the method by which the BIO X operates. This was rectified in future experiments with a 'test' check of the BIO X before use, making sure that the UV module correctly places itself above the centre of the μ -dish before printing. Gaining trust and understanding on how 3D printers operate, and methods to overcome the presence of such issues present a challenge to researchers when bioprinting.

4.4 Future Considerations

The fact that bioprinters hold promise, one day, to bring about transformative change in many aspects of biomedical science is one that cannot be denied. The ability to construct multi-layer models of biology may not be possible by other means. The precise deposition of material possible, via the G-code, could have many uses in cellular migration studies and the development of disease models. One could imagine a point where a bioprinter could create a basic biological model. Subsequent manipulation and the introduction of chemical cues could allow a more intricate representation of biology to develop, by which aspects of a model system or a specific disease could be studied. Models such as these may even serve as the potential platform for a drug development processes or patient-personalised models.

The current workflow presents a method for many imaging solution possibilities can be achieved and allows the incorporation of other crosslinking methods such as enzyme-mediated and temperature related processes. Further testing on constructs could involve drug treatments to see how cells respond in 3D *in vitro* environments.

The highly custom nature of the mechanical testing possible with the DHR-2 is a potential source of many future customisations. Many attachments are available for use with this instrument. The XHATCH 20 mm parallel plate was very useful for gripping the hydrogel for rheology analysis, avoiding the use of gripping materials such as sandpaper. The plate does not need to be this size however, a smaller plate such as 8 mm would have been highly preferred. This is due largely in part to the cost and the limited associated with the Laminink, production of a 20 mm size required a large volume of material to be used (approximately 0.5 mL

for each rheology disc). The ability to produce a smaller disc size, whilst providing the same quality of analysis, would allow less material to be used, saving on cost. The throughput rate of disc production would also be improved upon by lowering the printing time as a result of this. Therefore, use of a smaller peltier plate, such as the 8 mm supplied by TA instruments would improve many aspects of this workflow. Decreasing the volume of material required for rheological analysis provides the clear benefits of cost saving and the rate at which samples can be produced. Of particular interest in decreasing the size of the rheological disc to 8 mm would be to also gain the ability to perform analysis using a TA TX Texture Analyser, an additional instrument capable of providing data on the mechanical properties of hydrogels. Rheological testing was performed at 25 °C but in future testing at 37 °C would be more suited for hydrogel assessment as this is the temperature at which *in vivo* conditions are replicated. Waiting for temperature adjustment on the rheometer analysis would have to be incorporated into the workflow.

The presence of air bubbles within cell-laden hydrogels is a known issue that occurs during mixing procedures. This was experienced during the cell-laden Laminink preparation. Centrifugation is a method that was not performed due to the lack of an instrument that could hold the 3ml cartridges. However, this would be advised for any and all future hydrogel workups.

Looking at the workflow, a number of improvements to its design can be suggested. The first issue would be to methods to maintain sterility throughout. Cell preparation and bioprinting involved sample transfer between locations during this thesis and it would be well suited instead to have cell preparation and the BIO X within the same environment. In this setting, an incubator would be at hand. This would be useful as after printing, getting the cells incubated and brought to *in vivo* temperatures would limit the stress they are under. It was fortunate that a portable incubator (INCU-Line IL10) could be used alongside the BIO X. Whilst the BIO X itself is capable of maintaining a sterile environment with the use of its interior fans, ensuring that the immediate post-processing steps such as the ionic crosslinking and PBS washing are performed in fume cabinets are important in improving the sterility of the final bioprinted constructs.

The presence of FDM and resin printers were essential in troubleshooting during this thesis and as such they are recommended in pursuing development in any future bioprinting protocols. FDM printers are useful in the production of calibration plates and containers for materials while the Formlabs printer used for the static helix mixer design is essential in the creation of biomedical devices. The Biomed resin used by this machine can produce autoclavable components and while not explored fully in this thesis, alternative static mixers designs were pursued for a time to improve upon the cell encapsulation mixing process. The collagen

mold for example, was made using FDM methods. This is not ideal, instead making this design should be made using the Formlabs resin printer and Biomed medical grade resin. This was not performed due to time constraints.

Also introduced to the author was the potential of design improvements to 3D bioprinters. Calibrations are an area that could be improved upon. As seen in section 2.2.5 step 1.f, a number of calibrations are required. Aside from the required auto-bed levelling process the others had to be manually performed. Adjustments to this process could certainly be made. The manual placement of the nozzle and calibrating the z-height is entirely susceptible to human prone error for example. A 3D printed design for the BIO X, specific to the μ -dish or any other hardware used may improve upon any potential human error.

Another area would be a proper UV crosslinking guide, with an experimentally determined value for mW/mm^2 . This would give to any future results a value at which the crosslinking strength of UV provided to the hydrogels can be established, compared and used for future development.

During Laminink printing, as mentioned, maintaining the flow rate manually showed itself to be a major challenging in bioprinting. Increments of 1 kPa in either direction were often observed to be too high or low resulting in a poor flow rate of material. The possibility for smaller changes in pressure would be advantageous. Additionally, that the kPa changes were made via a touchscreen-LED may not have been the optimal and it would be interesting to see the inclusion of handheld controllers to maintaining flow rates during bioprinting.

It is clear that significant hurdles remain and more scientific progress will be achieved in this field when access to the right materials improves. FDM 3D printers are capable of holding 2 kg of plastic on spools, and some light-based resin tanks can hold 1 litre of printable material. In order to perform prototyping and perform larger studies bioprinters require the ability to handle increased capacity. Such scaling improvements are required in all aspects in future bioprinter design. The capsules currently available for the BIO X are by no means optimal. Improvements on this have to be made in order to produce multiple printed hydrogel constructs for imaging and mechanical testing.

It must also be considered that the method for incorporating cells, specifically spheroids and potentially organoids, performed in this workflow is not the way forward. That spheroids are able to seemingly drop out of the hydrogels whilst in the bioprinter is not ideal for the production of homogenous spheroid-containing hydrogels. Potentially the development of a method in which spheroids, or organoids, are inserted into a bioprinted construct during printing is the way forward. Considering this also needs to consider the nature of the machines at hand. Bioprints would have to be paused mid-print, cells inserted, and then restarted. Such a method may be the way towards spheroid- and organoid-encapsulated constructs.

In summary, the development of a bioprinting material is a multi-year process. Ideally, an in-house material would need to be developed, and that material would need to be guided through a journey of printability prototyping and model design which is a self-explained extensive process. Purchasing pre-made, ready to go material is not ideal, as it takes time to understand the nature of material enough for it to be printed correctly. Alternative visions for future study therefore may be the development of a bulk material which can be readily functionalised with the externally added components required to realise an *in vivo* tissue mimic.

With all the above said, it should be clear to researchers that wish to aspire to the development of a new, exciting innovation *in vitro* 3D cancer models open to studying many cellular types and eventually personalised drug treatments that the scope of the work involved can be considered as immense. With that being said, it is also true that many hands make light work and a concerted effort into the development of such a process can be achieved when many people are focussed on the same subject.

All in all, bioprinting is a complex process, but the potential gains to be made are significant. Intensive experimentation and optimisation is required to achieve the reality that is a fully realised bioprinting workflow.

Chapter 5

Conclusion

This workflow has shown to future researchers an insight into the bioprinting process, and how perform simultaneous imaging and mechanical testing of prototype hydrogel constructs. This workflow has brought to light many of the considerations that would have to be realised in the development of a process that may lead to the development of a hydrogel material for pancreatic cancer research.

The ability to image and gain data on cell viability and the matrix stiffness of hydrogels made using a BIO X 3D bioprinter has been established. A method for which spheroids grown may survive bioprinting has been demonstrated.

Collagen hydrogels act as a suitable platform for the study of pancreatic cancer cells in 3D. The process by which collagen hydrogels were formed from a mold presents an innovative new technique for which future studies can be performed on this material.

Laminink 411 has demonstrated itself as a bioprinting material that sets a high standard in the pursuit of an ideal hydrogel for the study of pancreatic cancer. The PANC-1 cellular clusters observed show high cell compatibility with this transparent material, and the fact they were seen to develop after repetition of the workflow on day-7 shows a strong resilience for this material to undergo continued testing. Although issues were experienced with printability and crosslinking, access to additional material would potentially eliminate any user errors and allow further optimisations to take place.

The numerous qualities of Laminink therefore establish this material as an important benchmark in the development of hydrogels designed for progressing 3D pancreatic cancer research. Future research guided towards the development of hydrogels capable of emulating such qualities will provide researchers with an important additional materials capable of offering further insights into the nature of cancer biology through innovative 3D model systems.

References

- [1] Lin CC, Korc M. Designer hydrogels: Shedding light on the physical chemistry of the pancreatic cancer microenvironment. *Cancer Lett.* 2018;436:22-7.
- [2] Mizrahi JD, Surana R, Valle JW, Shroff RT. Pancreatic cancer. *Lancet.* 2020;395(10242):2008-20.
- [3] Ho WJ, Jaffee EM, Zheng L. The tumour microenvironment in pancreatic cancer - clinical challenges and opportunities. *Nat Rev Clin Oncol.* 2020;17(9):527-40.
- [4] Monteiro MV, Ferreira LP, Rocha M, Gaspar VM, Mano JF. Advances in bioengineering pancreatic tumor-stroma physiomi-metic Biomodels. *Biomaterials.* 2022;287:121653.
- [5] Chakraborty S, Baine MJ, Sasson AR, Batra SK. Current status of molecular markers for early detection of sporadic pancreatic cancer. *Biochim Biophys Acta.* 2011;1815(1):44-64.
- [6] Kim M, Hwang DG, Jang J. 3D Pancreatic Tissue Modeling in vitro: Advances and Prospects. *BioChip Journal.* 2020;14(1):84-99.
- [7] Salinas-Vera YM, Valdes J, Perez-Navarro Y, Mandujano-Lazaro G, Marchat LA, Ramos-Payan R, et al. Three-Dimensional 3D Culture Models in Gynecological and Breast Cancer Research. *Front Oncol.* 2022;12:826113.
- [8] Liu HY, Greene T, Lin TY, Dawes CS, Korc M, Lin CC. Enzyme-mediated stiffening hydrogels for probing activation of pancreatic stellate cells. *Acta Biomater.* 2017;48:258-69.
- [9] Totti S, Allenby MC, Dos Santos SB, Mantalaris A, Velliou EG. A 3D bioinspired highly porous polymeric scaffolding system for in vitro simulation of pancreatic ductal adenocarcinoma. *RSC Adv.* 2018;8(37):20928-40.
- [10] Farooque TM, Camp CH, Jr., Tison CK, Kumar G, Parekh SH, Simon CG, Jr. Measuring stem cell dimensionality in tissue scaffolds. *Biomaterials.* 2014;35(9):2558-67.
- [11] Pradhan S, Clary JM, Seliktar D, Lipke EA. A three-dimensional spheroidal cancer model based on PEG-fibrinogen hydrogel microspheres. *Biomaterials.* 2017;115:141-54.
- [12] Nguyen EH, Zanutelli MR, Schwartz MP, Murphy WL. Differential effects of cell adhesion, modulus and VEGFR-2 inhibition on capillary network formation in synthetic hydrogel arrays. *Biomaterials.* 2014;35(7):2149-61.
- [13] Monteiro MV, Zhang YS, Gaspar VM, Mano JF. 3D-bioprinted cancer-on-a-chip: level-up organotypic in vitro models. *Trends Biotechnol.* 2022;40(4):432-47.
- [14] CELLINK. BIO X 2023 [Available from: <https://www.cellink.com/product/bio-x/?country=NO>].

- [15] Simińska-Stanny J, Nizioł M, Szymczyk-Ziółkowska P, Brożyna M, Junka A, Shavandi A, et al. 4D printing of patterned multimaterial magnetic hydrogel actuators. *Additive Manufacturing*. 2022;49.
- [16] Shen J, Zhang S, Fang X, Salmon S. Advances in 3D Gel Printing for Enzyme Immobilization. *Gels*. 2022;8(8).
- [17] Lin CC, Anseth KS. PEG hydrogels for the controlled release of biomolecules in regenerative medicine. *Pharm Res*. 2009;26(3):631-43.
- [18] Jiang Y, Chen J, Deng C, Suuronen EJ, Zhong Z. Click hydrogels, microgels and nanogels: emerging platforms for drug delivery and tissue engineering. *Biomaterials*. 2014;35(18):4969-85.
- [19] Gonzalez-Fernandez T, Tenorio AJ, Campbell KT, Silva EA, Leach JK. Alginate-Based Bioinks for 3D Bioprinting and Fabrication of Anatomically Accurate Bone Grafts. *Tissue Eng Part A*. 2021;27(17-18):1168-81.
- [20] Kostenko A, Connon CJ, Swioklo S. Storable Cell-Laden Alginate Based Bioinks for 3D Biofabrication. *Bioengineering (Basel)*. 2022;10(1).
- [21] Kozłowski MT, Crook CJ, Ku HT. Towards organoid culture without Matrigel. *Commun Biol*. 2021;4(1):1387.
- [22] Raza A, Ki CS, Lin CC. The influence of matrix properties on growth and morphogenesis of human pancreatic ductal epithelial cells in 3D. *Biomaterials*. 2013;34(21):5117-27.
- [23] CELLINK. GelXA Laminink 411 2023 [Available from: <https://www.cellink.com/product/gelxa-laminink-411/>].
- [24] Wu DT, Diba M, Yang S, Freedman BR, Elosegui-Artola A, Mooney DJ. Hydrogel viscoelasticity modulates migration and fusion of mesenchymal stem cell spheroids. *Bioeng Transl Med*. 2023;8(3):e10464.
- [25] Kaido T, Yebra M, Cirulli V, Montgomery AM. Regulation of human beta-cell adhesion, motility, and insulin secretion by collagen IV and its receptor alpha1beta1. *J Biol Chem*. 2004;279(51):53762-9.
- [26] Weber LM, Hayda KN, Haskins K, Anseth KS. The effects of cell-matrix interactions on encapsulated beta-cell function within hydrogels functionalized with matrix-derived adhesive peptides. *Biomaterials*. 2007;28(19):3004-11.
- [27] Below CR, Kelly J, Brown A, Humphries JD, Hutton C, Xu J, et al. A microenvironment-inspired synthetic three-dimensional model for pancreatic ductal adenocarcinoma organoids. *Nat Mater*. 2022;21(1):110-9.
- [28] Daoud JT, Petropavlovskaja MS, Patapas JM, Degrandpre CE, Diraddo RW, Rosenberg L, et al. Long-term in vitro human pancreatic islet culture using three-dimensional microfabricated scaffolds. *Biomaterials*. 2011;32(6):1536-42.
- [29] Nwaneshiudu A, Kuschal C, Sakamoto FH, Anderson RR, Schwarzenberger K, Young RC. Introduction to confocal microscopy. *J Invest Dermatol*. 2012;132(12):e3.
- [30] Rice AJ, Cortes E, Lachowski D, Cheung BCH, Karim SA, Morton JP, et al. Matrix stiffness induces epithelial-mesenchymal transition and promotes chemoresistance in pancreatic cancer cells. *Oncogenesis*. 2017;6(7):e352.

- [31] Rubiano A, Delitto D, Han S, Gerber M, Galitz C, Trevino J, et al. Viscoelastic properties of human pancreatic tumors and in vitro constructs to mimic mechanical properties. *Acta Biomater.* 2018;67:331-40.
- [32] Shan J, Chi Q, Wang H, Huang Q, Yang L, Yu G, et al. Mechanosensing of cells in 3D gel matrices based on natural and synthetic materials. *Cell Biol Int.* 2014;38(11):1233-43.
- [33] Hina A. Modelling 3D Cancer Growth and Extracellular Matrix Properties In Vitro. Stavanger: University of Stavanger; 2018.
- [34] CELLINK. Bioprinting Protocol GelXA LAMININK. 2023.
- [35] CELLINK. How to install HeartWare 2021 [Available from: <https://cellink.freshdesk.com/support/solutions/articles/35000147419-step-1-how-to-install-heartware-bioprinting-assisting-software-on-a-windows-pc-bio-x>].
- [36] Yin J, Yan M, Wang Y, Fu J, Suo H. 3D Bioprinting of Low-Concentration Cell-Laden Gelatin Methacrylate (GelMA) Bioinks with a Two-Step Cross-linking Strategy. *ACS Appl Mater Interfaces.* 2018;10(8):6849-57.
- [37] CELLINK. CELLINK 405nm Crosslinking Module Data Specifications 2020 [Available from: <https://cellink.freshdesk.com/support/solutions/articles/35000071261-cellink-405nm-crosslinking-module-s-data-specifications>].

Appendix

Calculations

1. Collagen Hydrogel Preparation

	TeloCol-10 (Collagen Stock)		Collagen + PBS		Collagen + PBS + HEPES		Cell-Laden Collagen
	C_1V_1		C_2V_2		C_3V_3		C_4V_4
Concentration (mg/mL)	10.2	1. Dilute w/ PBS	6.6	2. Buffer w/ HEPES	3.3	3. Add cell- solution	3.0
Volume (μ L)	1456	(796 μ L)	2250	(2250 μ L)	4500	(500 μ L)	5000

Figure 1. Collagen hydrogel calculation example; showing preparation of a 5 mL solution of 3 mg/ml cell-laden collagen hydrogel containing 2D cultured PANC-1 cells at a ratio of 1:10.

All collagen hydrogel work-ups were performed in a cold-room. All solutions were placed on ice prior to mixing. Mixing was performed within a glass beaker. After step 2 (addition of 100 mM HEPES), collagen solutions were transferred to a BD Plastipak syringe and kept in a fridge at 4 °C until use in cell encapsulations.

2. Cell Counting

$$\frac{\text{Total Cell Number (\#)}}{\text{Viable Cells / mL}} \times 1000 = \text{Volume (\mu L) of Cell Solution Required}$$

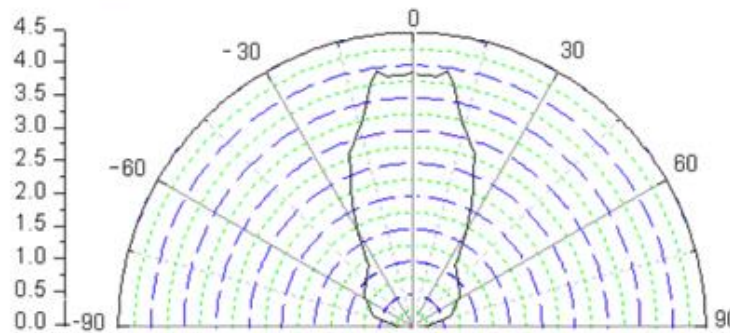
Figure 2. Cell solution volume calculation. Viability checks performed using the Muse gained a value for the 'viable cells / ml' in the cell solution extracted from the standard 2D cell culture flasks. This was used to calculate the volume of cell solution required to be added to the hydrogel base materials and for preparing hanging drop spheroids and spheroids grown in microwell plates (for 3D spheroid preparations, 10,000 cells were suspended in 40 μ L cell media).

3. 405 nm Crosslinking Guide

CELLINK supplies the following information online relating to their 405 nm UV module on the BIO X (figure 3 and 4) [37].

Parameter	Symbol	Min.	Typ.	Max	Unit	Condition
Radiant Flux	Φ_e	900	---	---	mW	IF=500mA
Forward Voltage	VF	3	---	3.6	V	
Peak Wavelength	λ_p	---	405	---	nm	
Viewing Angle	$2\theta_{1/2}$	---	50	---	deg	

Figure 3. Optoelectrical parameters of BIO X 405 nm UV module at 60 mm nominal distance to surface.



Notes:

1. $2\theta_{1/2}$ is the off axis angle from lamp centerline where the luminous intensity is 1/2 of the peak value.
2. View angle tolerance is $\pm 5^\circ$.

Figure 4. Radiation diagram of BIO X 405 nm UV module.

Radiant flux, the parameter in figure 3, is defined as the radiant energy emitted, reflected, transmitted or received per unit time. Unit time is one second, and since the distance to the surface is given as 60 mm, it can be assumed that this UV module has a radiant flux of 900 mW/s at a distance of 60 mm.

The radiant diagram is a form of polar plot. The black line is the intensity of light emitted as a function of beam angle. The following information was extracted from figure 4.

- It is stated that the 'off axis angle' from lamp centreline has a luminous intensity 1/2 of the peak value.
- The line of highest relative luminous intensity occurs at approximately 3.875, at an angle of 8° .
- Therefore, for this LED, everything $<8^\circ$ experiences 100%, and $>8^\circ$ experiences $<100\%$.
- At 8 degrees, the surface intensity is 100%
- At 10 degrees, the surface intensity is 96%
- At 12 degrees, the surface intensity is 90%
- At 15 degrees, the surface intensity is 77%

An accurate diagram of a ruler printed on A4 paper, cut out and transferred to the BIO X. Images of the BIO X 405 nm module beam diameter were taken so that they could be measured.

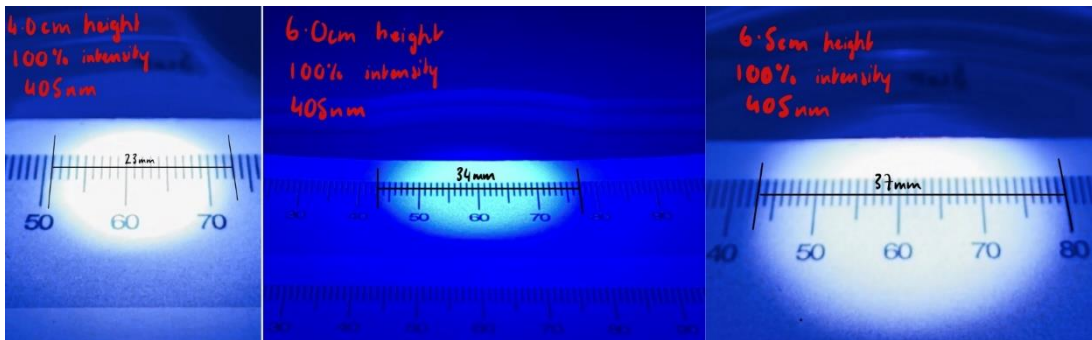


Figure 5. BIO X 405 nm beam diameters at 4.0, 6.0 and 6.5 cm height. Beam diameters measured: 4.0 cm - 23 mm; 6.0 cm - 34 mm; 6.5 cm - 37 mm.

It was thought necessary to further define the beam, to elucidate further on the relationship between UV module height, intensity and beam diameter. Using the images and measurements taken (figure 5). The following image was constructed within the CAD software Blender.

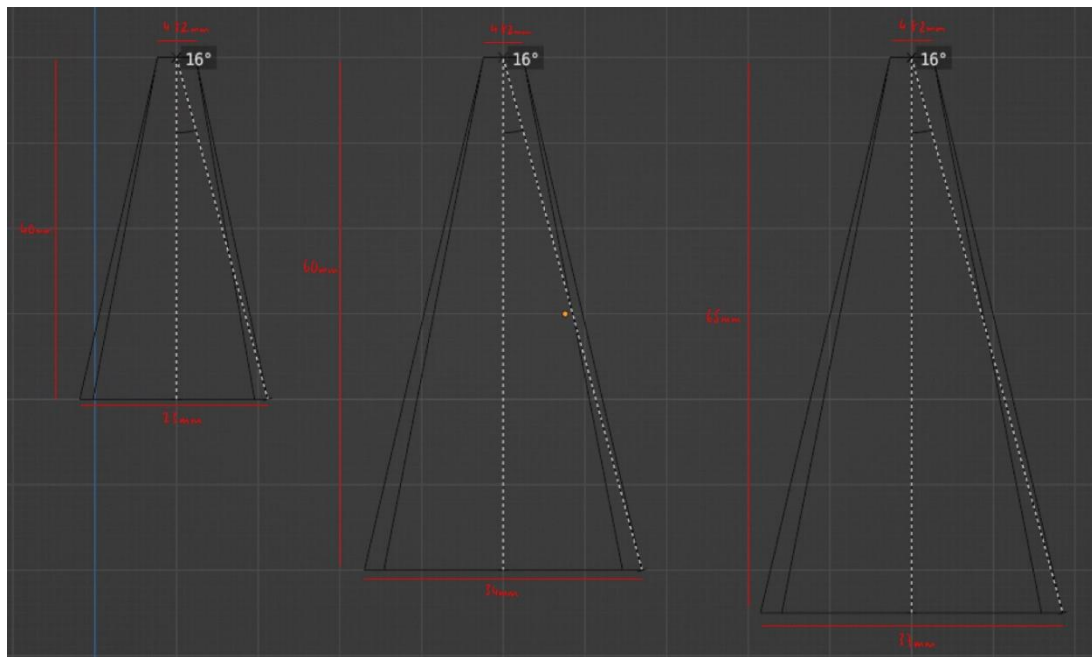


Figure 6. BIO X 405 nm beams created in Blender at 4.0, 6.0 and 6.5 cm module height. The angle at which the edge of the beam occurs was determined to be 16° .

The edge of the beam was calculated to be 16° . Thus, at an angle of 16° the beam diameters are 23, 34 and 37 mm corresponding to the heights of 4, 6 and 6.5 cm respectively. Calculating the beam diameter at 8° , identified in the radiation diagram as the point at which everything under this value has 100% intensity was used to produce the following (figure 7).

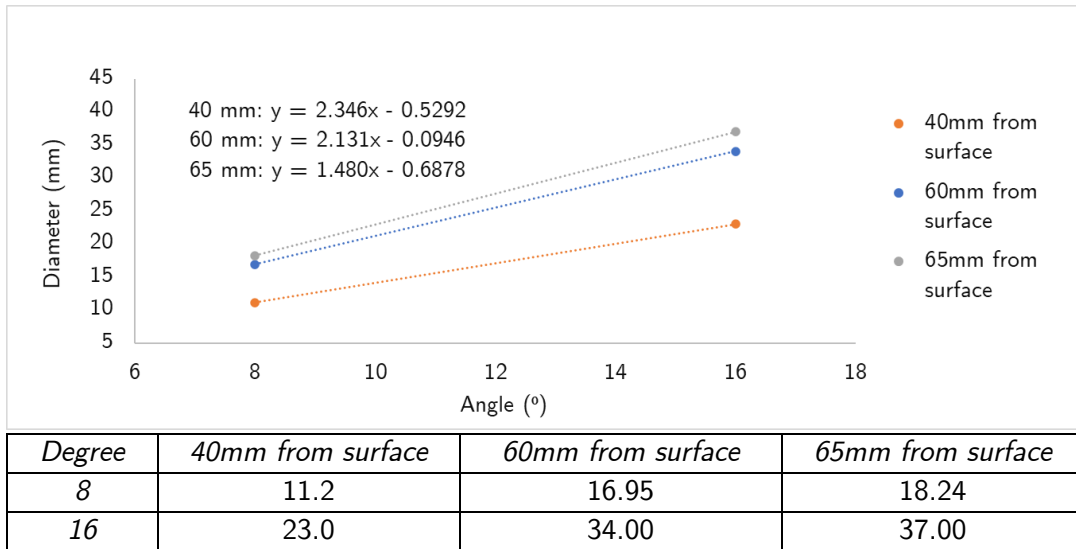


Figure 7. Beam surface area on BIO X with beam angles of 8 and 16 degrees.

Therefore, between the heights of 40 to 65 mm (which is the total allowed changeable height allowed in the BIO X hardware) there are three equations that can define beam surface area on the BIO X. Combining the radiation diagram intensity information with the beam angle allows the following to be produced (figure 8).

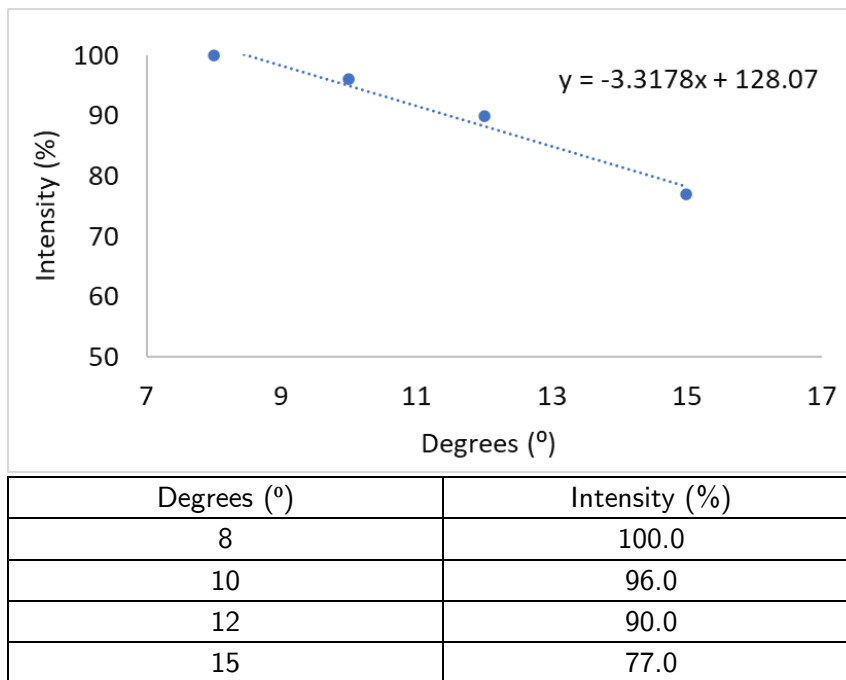


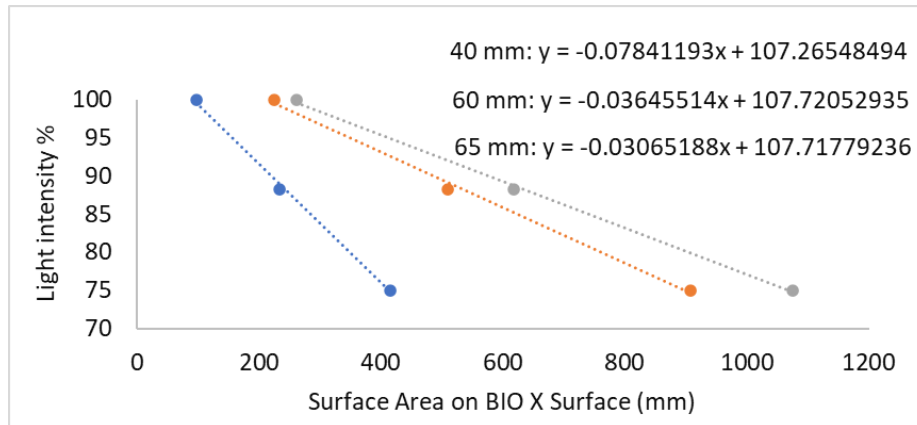
Figure 8. Intensity of emitted light as a function of degree angle.

The surface area within the beams at angles 8, 12, and 16 produce on the surface of the BIO X were also calculated (table 1).

Table 1. Calculated surface areas within certain beam angles.

Height (mm)	8° Diameter	8° Surface Area	12° Diameter	12° Surface Area	16° Diameter	16° Surface Area
40	11.2	97.75	17.24	233.53	23.00	415.48
60	17.0	225.72	25.48	510.02	34.00	907.92
65	18.2	261.17	28.06	618.21	37.00	1075.21

The slope obtained from the equation in figure 8 can be combined with the data in table 1 to produce the following (figure 9).



	<i>Degree (°)</i>	8.0	12	16
40	<i>Intensity %</i>	100.0	88.3	75.0
	<i>Surface area (mm)</i>	97.7	233.5	415.5
60	<i>Intensity %</i>	100.0	88.3	75.0
	<i>Surface area (mm)</i>	225.7	510.0	907.9
65	<i>Intensity %</i>	100.0	88.3	75.0
	<i>Surface area (mm)</i>	261.2	618.2	1075.2

Figure 9. Relating beam angle, intensity and surface area.

Combining the slopes from the straight-line equations obtained in figure 9 allowed the following graph to be produced (figure 10).

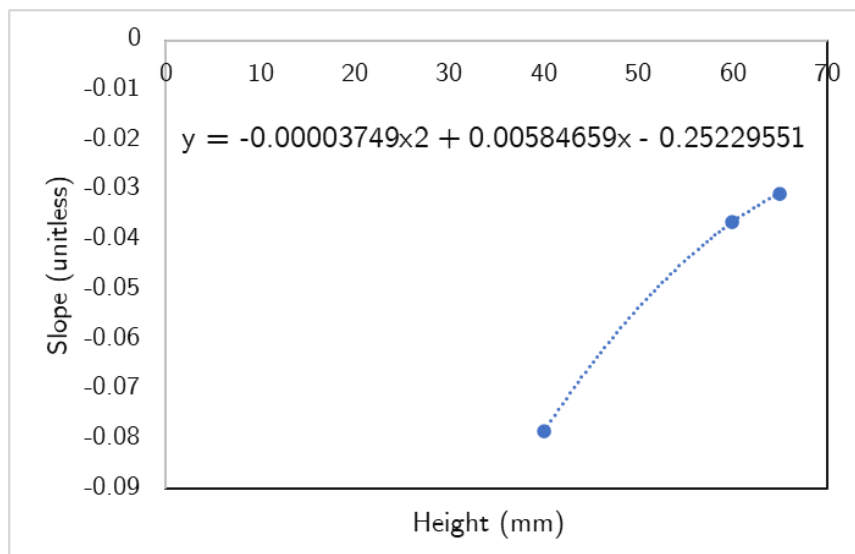


Figure 10. Relationship between 405 nm UV module height and light intensity.

Figure 10 relates the height to the slope gradient (obtained in figure 9), this can be used to determine the light intensity based on the surface area. Using the specifications provided by CELLINK we can determine the following:

- Energy that each mm² of surface area of a hydrogel construct receives
- Radiant flux at each height with the beam angle considered

CELLINK states that at 60 mm nominal height the radiant flux is 900 mW. Additionally, we know that the surface area of our construct is 314 mm² (20 mm diameter). Using the Light Inverse Square Law, which states “the intensity of light changes in inverse proportion to the square of the distance from the source”, we can calculate how the radiant flux changes with height. Combining this with the polynomial equation obtained in figure 10, we are now able to calculate, theoretically, the % intensity of light based on the surface area. The extend of the table produced to calculate this is too large to be contained within this document format.

Table 2. Scaled down version of table used to calculate mW/mm².

Height	40.0		...	60		...	65	
Light Intensity Equation	-0.078	Radiant Flux	...	-0.036	Radiant Flux	...	-0.030	Radiant Flux
314.0	82.6	1673.6	...	95.8	862.4	...	97.6	748.8
313.0	82.7	1675.2	...	95.9	862.7	...	97.7	749.0
...
239.0	88.5	1792.7	...	98.6	887.0	...	99.9	766.4
238.0	88.6	1794.3	...	98.6	887.3	...	100.0	766.9
237.0	88.7	1795.9	...	98.6	887.7	...	100.0	766.9
...
201.0	91.5	1853.0	...	99.9	899.5	...	100.0	766.9
200.0	91.6	1854.6	...	100.0	900.0	...	100.0	766.9
199.0	91.7	1856.2	...	100.0	900.0	...	100.0	766.9
...
94.0	99.9	2023.0	...	100.0	900.0	...	100.0	766.9
93.0	100.0	2025.0	...	100.0	900.0	...	100.0	766.9
92.0	100.0	2025.0	...	100.0	900.0	...	100.0	766.9
...
2.0	100.0	2025.0	...	100.0	900.0	...	100.0	766.9
1.0	100.0	2025.0	...	100.0	900.0	...	100.0	766.9
Average	93.6	1900.6	...	99.2	893.1	...	99.7	764.6

In table 2, the dots (“...”) represent the presence of data extending between adjacent cells. This is how the crosslinking guide was created (table 3). Highlighted in purple is the 900 mW provided by CELLINK, which was used to infer all other

results. Yellow highlighted cells represent the 100% intensity boundary. Examples of the data that can be extracted from this graph are the following:

- At 60 mm, a UV module shines 100% intensity on a surface area of 200 mm². A surface area of 201 mm² experiences 99.9% intensity.
- At 40 mm, at surface area 314 mm², the intensity of light upon this outer area of the circle is 82.6 %. Increasing this to 65 mm height, the beam diameter expands resulting in 97.6 % of intensity reaching this area. However, due to the inverse square law the radiant flux between these two heights are very different, showing 1673.6 and 748.8 respectively.

Table 3. Highlighted version of BIO X 405 nm crosslinking guide.

Height (mm)	Average Intensity on a Surface Area of 314mm ²	Average Radiant Flux on a Surface Area of 314mm ²	Radiant Flux (mW/mm ² ·s)
40	93.9	1900.6	5.90
41	94.3	1816.8	5.64
42	94.6	1738.5	5.40
43	95.0	1665.1	5.17
44	95.4	1596.3	4.96
45	95.7	1531.7	4.76
46	96.1	1471.0	4.57
47	96.4	1413.7	4.39
48	96.7	1359.7	4.22
49	97.0	1308.7	4.06
50	97.3	1260.5	3.91
51	97.5	1214.8	3.77
52	97.8	1171.5	3.64
53	98.0	1130.4	3.51
54	98.2	1091.3	3.39
55	98.4	1054.2	3.27
56	98.6	1018.8	3.16
57	98.8	985.1	3.06
58	98.9	953.0	2.96
59	99.1	922.4	2.86
60	99.2	893.1	2.77
61	99.4	865.1	2.69
62	99.5	838.3	2.60
63	99.6	812.7	2.52
64	99.6	788.1	2.45
65	99.7	764.6	2.37

The above guide was highly theoretical in nature and does by no means accurately represent the reality of the mW/mm² of energy transferred to the hydrogel constructs. It was created in order to give the author an ability to provide some reference to the UV-mediated crosslinking of hydrogel constructs.